Geophys. J. Int. (2004) **157,** 607–628 doi: 10.1111/j.1365-246X.2004.02195.x

Shear wave velocity, seismic attenuation, and thermal structure of the continental upper mantle

Irina M. Artemieva,[1,2] Magali Billien,[2] Jean-Jacques Lévêque[2] and Walter D. Mooney[1]

[1] *USGS, MS* 977, 345 *Middlefield Road, Menlo Park, CA* 94025*, USA.*
E-mails: Irina.Artemieva@eost.u-strasbg.fr (IMA); Mooney@usgs.gov (WDM)
[2] *Ecole et Observatoire de Sciences de la Terre,* 5 *rue René Descartes, Strasbourg cedex* F-67084*, France.*
E-mails: Magali.Billien@eost.u-strasbg.fr (MB); JeanJacques.Leveque@eost.u-strasbg.fr (JJL)

Accepted 2003 November 7. Received 2003 November 1; in original form 2003 January 7

SUMMARY

Seismic velocity and attenuation anomalies in the mantle are commonly interpreted in terms of temperature variations on the basis of laboratory studies of elastic and anelastic properties of rocks. In order to evaluate the relative contributions of thermal and non-thermal effects on anomalies of attenuation of seismic shear waves, Q_s^{-1}, and seismic velocity, V_s, we compare global maps of the thermal structure of the continental upper mantle with global Q_s^{-1} and V_s maps as determined from Rayleigh waves at periods between 40 and 150 s. We limit the comparison to three continental mantle depths (50, 100 and 150 km), where model resolution is relatively high.

The available data set does not indicate that, at a global scale, seismic anomalies in the upper mantle are controlled solely by temperature variations. Continental maps have correlation coefficients of <0.56 between V_s and T and of <0.47 between Q_s and T at any depth. Such low correlation coefficients can partially be attributed to modelling artefacts; however, they also suggest that not all of the V_s and Q_s anomalies in the continental upper mantle can be explained by T variations.

Global maps show that, by the sign of the anomaly, V_s and Q_s usually inversely correlate with lithospheric temperatures: most cratonic regions show high V_s and Q_s and low T, while most active regions have seismic and thermal anomalies of the opposite sign. The strongest inverse correlation is found at a depth of 100 km, where the attenuation model is best resolved. Significantly, at this depth, the contours of near-zero Q_s anomalies approximately correspond to the 1000 °C isotherm, in agreement with laboratory measurements that show a pronounced increase in seismic attenuation in upper mantle rocks at 1000–1100 °C. East–west profiles of V_s, Q_s and T where continental data coverage is best (50°N latitude for North America and 60°N latitude for Eurasia) further demonstrate that temperature plays a dominant, but non-unique, role in determining the value of lithospheric V_s and Q_s.

At 100 km depth, where the resolution of seismic models is the highest, we compare observed seismic V_s and Q_s with theoretical V_s^T and Q_s^T values, respectively, that are calculated solely from temperature anomalies and constrained by experimental data on temperature dependencies of velocity and attenuation. This comparison shows that temperature variations alone are sufficient to explain seismic V_s and Q_s in *ca* 50 per cent of continental regions. We hypothesize that compositional anomalies resulting from Fe depletion can explain the misfit between seismic and theoretical V_s in cratonic lithosphere. In regions of active tectonics, temperature effects alone cannot explain seismic V_s and Q_s in the lithosphere. It is likely that partial melts and/or fluids may affect seismic parameters in these regions. This study demonstrates that lithospheric temperature plays the dominant role in controlling V_s and Q_s anomalies, but other physical parameters, such as compositional variations, fluids, partial melting and scattering, may also play a significant role in determining V_s and Q_s variations in the continental mantle.

Key words: composition, cratons, lithosphere, partial melts, Rayleigh waves, temperature.

1 INTRODUCTION

It is widely accepted that a significant part of lateral variations in seismic velocity and attenuation anomalies in the mantle can be attributed to temperature variations. Other possible causes of seismic anomalies include compositional variations, partial melts and/or fluids. In the present study we examine the correlations between seismic shear wave velocities (V_s), inverse attenuation (Q_s) and temperature (T) in order to distinguish non-thermal and thermal origins of seismic anomalies in the continental uppermost mantle. Our special interest is to gain a better understanding of the physical nature of attenuation anomalies, because some recent interpretations of mantle attenuation assume that compositional variations in the mantle and/or the presence of partial melt have little effect on anelasticity and thus can be ignored (Nakajima & Hasegawa 2003). Numerous seismic and laboratory studies have addressed the question of the correlation between seismic elastic and anelastic properties, and temperatures.

1.1 The correlation between seismic velocity and attenuation

Anelasticity is manifested by the attenuation of the amplitude of waves during their propagation and is generally quantified in seismology by the quality factors, Q_p and Q_s, for compressional and shear waves, respectively. Global anelastic tomography studies (e.g. Romanowicz & Durek 2000) as well as regional seismic studies for the oceans (e.g. Sheehan & Solomon 1992) found that anomalies of seismic velocity and attenuation are correlated. Seismic studies of the Japan arc (Tsumura *et al.* 2000) demonstrated that low-Q zones in the upper mantle are well correlated with low-velocity zones beneath active volcanoes where partial melting is expected. A strong inverse correlation of tomographic elastic and anelastic models beneath 100 km depth in the Tonga–Fiji region was used to derive an exponential empirical relationship between two of the parameters and to constrain the physical state of the upper mantle (Roth *et al.* 2000). A similarity between the observed relationship and predictions based on experimental studies (e.g. Sato *et al.* 1989; Karato 1993), permitted the authors to conclude that both attenuation and velocity anomalies should be primarily of thermal origin (Roth *et al.* 2000).

1.2 The correlation between seismic velocity and temperature

The strong effect of temperature on seismic velocity and elastic moduli has long been known from laboratory studies (e.g. Ide 1937; Birch 1943; Hughes & Cross 1951), implying that velocity perturbations in the uppermost mantle can be partly the result of temperature variations. Most of measurements were made at relatively low temperatures (< 600–$700\,^{\circ}$C) (Fielitz 1971; Kern 1978; Christensen 1979) with very limited data available for $T > 1000^{\circ}$C (Berckhemer *et al.* 1982; Murase & Kushiro 1979; Murase & Fukuyama 1980; Sato *et al.* 1989; Jackson 1993). At high homologous temperatures T_m/T (where T_m is solidus temperature), a dependence of velocity on temperature is approximately linear with $\partial V_s/\partial T = 0.35$ m s^{-1} K^{-1} (Sumino & Anderson 1982); however, at near-solidus temperatures both V_p and V_s seismic velocities rapidly decrease with an increase of a percentage of melt (Fig. 1; Murase & Fukuyama 1980).

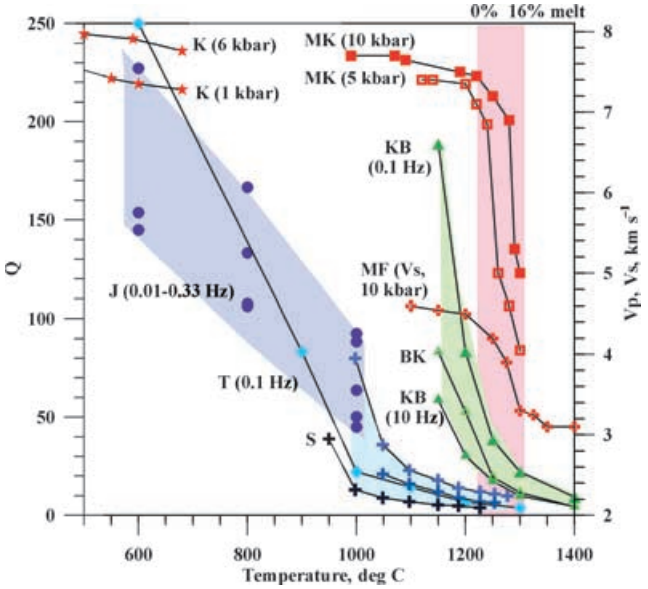

Figure 1. Experimental data on temperature dependence of Q, V_p and V_s. Purple dots and purple shading (J): Q in dunite at $P = 300$ MPa, $f = 0.01$–0.33 Hz (Jackson *et al.* 1992). Blue crosses and shading (S): Q in dry peridotite at $P = 0.20, 0.48$, and 0.73 GPa measured at ultrasonic frequencies (Sato & Sacks 1989). Green triangles and shading (BK, KB): Q in dunite at $f = 0.1$ and 10 Hz (Berckhemer *et al.* 1982; Kampfmann & Berckhemer 1985). Light blue rhombs (T): Q in olivine aggregate at $f = 0.09$ Hz (Tan *et al.* 1997). Red symbols: seismic velocities in peridotite. Stars (K): V_p at $P = 1$ and 6 kbar (Kern 1978). Rectangles (MK): V_p at $P = 5$ and 10 kbar (Murase & Kushiro 1979). Crosses (MF): V_s at $P = 10$ kbar (Murase & Fukuyama 1980). Pink shaded area: the region where volume fraction of melt in peridotite increases from 0 to 16 per cent at $P = 10$ kbar (Murase & Fukuyama 1980). At high temperatures, the effect of T on Q_s and V_s is different: a sharp increase in Q_s occurs at a lower temperature than a drop in V_s associated with partial melting.

High sensitivity of seismic velocities to temperature variations provides important constraints on the thermal regime of the upper mantle and has been successfully applied to estimate temperature variations in the upper mantle of Europe (Furlong *et al.* 1995; Sobolev *et al.* 1996; Goes *et al.* 2000) and North America (Goes & van der Lee 2002) from regional seismic tomography models. However, conversions of observed seismic velocities to temperatures should be treated with caution because non-thermal effects (resulting from compositional variations or the presence of melts/fluids) on seismic velocity variations are difficult to quantify (see Sections 3 and 5 below).

1.3 The correlation between seismic attenuation and temperature

The strong effect of temperature on seismic attenuation has been measured in a number of experimental studies (Fig. 1). Laboratory measurements of seismic wave attenuation in ultramafic uppermantle rocks were carried out for a wide range of pressures and temperatures at ultrasonic frequencies (60–900 KHz) on dry peridotite (Sato *et al.* 1989), and at seismic frequencies (0.01–1 Hz) on dry dunite (Berckhemer *et al.* 1982; Jackson *et al.* 1992) and on synthetic polycrystalline olivine (Tan *et al.* 1997; Gribb & Cooper 1998; Jackson 2000; Jackson *et al.* 2002). They show that at seismic frequencies attenuation, Q^{-1}, in mantle rocks at subsolidus temperatures follows the Arrhenius law and exponentially increases with

temperature T:

$$Q^{-1} = A\tau^{\alpha}\exp(-\alpha E^{*}/RT), \quad (1)$$

where E^{*} is the activation energy, R is the gas constant, τ is the oscillation period, A is a scaling constant and the exponent α is approximately 0.15–0.30 as determined from seismic studies and laboratory measurements on the upper-mantle rocks (e.g. Jackson *et al.* 1992).

Laboratory measurements of the temperature dependence of seismic attenuation for olivine-rich rocks were used in a number of studies where mantle geotherms were calculated from seismic attenuation (e.g. Kampfmann & Berckhemer 1985; Sato *et al.* 1988; Sato & Sacks 1989; Karato 1990; Nakajima & Hasegawa 2003). However, attenuation values determined from laboratory studies (eq. 1) include only intrinsic (anelastic) attenuation, while global and regional seismological studies measure the sum of anelastic and scattering effects.

The high sensitivity of seismic attenuation to temperatures, revealed in laboratory measurements, was recently used to correlate seismic attenuation anomalies in the mantle with temperature variations (e.g. Durek *et al.* 1993; Romanowicz 1994; Mitchell 1995; Romanowicz 1995). Regional seismic studies of North Atlantic (Sheehan & Solomon 1992) and western Pacific subduction zones (Nakanishi 1978; Bodri *et al.* 1991; Tsumura *et al.* 2000) suggest that a significant part of attenuation anomalies in the oceanic upper mantle can be explained by temperature variations and partial melting. In a global study, Romanowicz (1995) found that in the depth interval from 100 to 300 km shear wave attenuation Q_s^{-1} calculated from the amplitudes of low-frequency Rayleigh waves on a $10^{\circ} \times 10^{\circ}$ grid (the QR19 model) correlates with the surface heat flow values (the correlation coefficient r is in the range 0.20 to 0.35 with the correlation peak at $z \sim 200$ km); while at depths of $z > 250$ km Q_s^{-1} correlates with the hot spot distribution, with the strongest correlation ($r \sim 0.35$–0.38) at $z \sim 300$–660 km. However, it is important to note that these correlations are based mostly on high attenuation anomalies documented for oceanic regions (mid-ocean ridges, the western Pacific subduction zones and the East Pacific Rise), but not for the continents.

On the continents, studies of seismic shear wave attenuation revealed a qualitative correlation between regional attenuation anomalies in the crust and upper mantle and tectonic provinces (e.g. Nakanishi 1978; Canas & Mitchell 1978; Roult 1982; Dziewonski & Steim 1983; Chan & Der 1988; Mitchell *et al.* 1997; Sarker & Abers 1998; Selby & Woodhouse 2002). Low seismic attenuation in the upper mantle has been reported beneath western Australia, western Africa and the Himalayas in a number of recent anelastic tomographic models (e.g. Romanowicz 1994, 1995; Bhattacharyya *et al.* 1996), supporting the idea of the thermal origin of most of the upper-mantle Q_s^{-1} anomalies.

Few studies have been carried out so far to analyse the correlations between all three parameters (V_s, Q_s and T) on the global scale. Here, we aim to evaluate the influence of T on V_s and Q_s for the continents and compare shear wave velocities and attenuation at different depths in the upper 150 km of the mantle with temperature estimates (Artemieva & Mooney 2001). The present work uses a new 3-D model of Q_s (Billien *et al.* 2000) with the maximum resolution at a depth of 100 km and the corresponding 3-D model of V_s (both Q_s and V_s are effectively degree-13 spherical harmonic; Billien 1999).

We first calculate global correlation coefficients between all pairs of the parameters and find that, though a large part of seismic anomalies correlates with T variations in the upper mantle, temperatures alone cannot explain the amplitudes of velocity and attenuation anomalies. We discuss other mechanisms responsible for V_s and Q_s variations and examine a qualitative correlation between V_s, Q_s and T maps for 50, 100 and 150 km depths for different tectonic provinces. We finally use experimental relationships between seismic parameters and temperature and calculate global maps of mantle attenuation and shear velocity predicted from temperatures. A comparison of these maps with the seismic maps permits the outlining of regions where mechanisms other than thermal should be involved to explain seismic anomalies.

2 METHODS FOR CALCULATING V_s, Q_s AND T IN THE UPPER MANTLE

2.1 Shear wave velocity and attenuation models

2.1.1 The data

Studies of seismic attenuation in the Earth's mantle using surface waves began with the works of Anderson & Archambeau (1964), Ben-Menahem (1965) and Anderson *et al.* (1965): however, global attenuation models have been calculated only recently (Romanowicz 1995; Bhattacharyya *et al.* 1996; Durek & Ekström 1996; Reid *et al.* 2001; Selby & Woodhouse 2002). Velocity and attenuation maps used in this study are based on surface waves that sample the Earth all along their path from the surface to deep upper mantle. Compared to body waves, which have poor sampling (especially in the oceans) and thus very poor vertical resolution in the upper mantle, surface waves provide good vertical resolution down to 200–300 km and have acceptable horizontal resolution for discussing large geological units.

In the present study, we use a subset of the 3-D upper-mantle V_s and Q_s models of Billien (1999) and Billien *et al.* (2000). The models are based on the inversion of broad-band seismological data of fundamental mode surface waves. The data used are amplitude and frequency spectra at periods between 40 and 150 s for the direct path Rayleigh wave data (the first orbit only), which is a subset of the extensive phase and amplitude data set measured and selected by Trampert & Woodhouse (2001). For a detailed description of the automatic measurement technique and implementation of the strict data rejection criteria, see Trampert & Woodhouse (1995).

2.1.2 Simultaneous inversion for shear wave velocity and attenuation

V_s and Q_s calculations are based on a two-step inversion (for details see Billien 1999; Billien *et al.* 2000). First, from phase (Φ) and amplitude (A) measurements, Billien *et al.* (2000) made a simultaneous regionalization of the phase velocity (c_R) and the surface wave attenuation factor ($q_R = Q_R^{-1}$) at several periods:

$$A_i(\omega), \Phi_i(\omega) \Rightarrow c_R(\omega, \theta, \phi), q_R(\omega, \theta, \phi). \quad (2)$$

A depth inversion of the phase velocities and surface wave attenuation maps at different frequencies provides a 3-D model of the shear wave velocity V_s and the shear wave attenuation factor $q_s (q_s = Q_s^{-1})$ (Billien 1999):

$$q_R(\omega, \theta, \phi) \Rightarrow q_s(z, \theta, \phi), \quad (3)$$

$$c_R(\omega, \theta, \phi) \Rightarrow V_s(z, \theta, \phi). \quad (4)$$

The classical inversion method of Tarantola & Valette (1982) is used at this stage. It employs a least-squares method and includes information on the expected model in the form of: (i) an *a priori* model and (ii) an *a priori* covariance of the model. Billien (1999) used a layered version of PREM with 50 km thick layers in the depth range 25–825 km as the *a priori* velocity and attenuation models. The upper 25 km (the crustal layer) are fixed to the PREM value and are never updated in the inversion process. In the globally spherical PREM model (Dziewonski & Anderson 1981) the radial average Q_s has a value of 600 at depths between 40 and 80 km, and $Q_s = 80$ between 80 and 220 km. Similar to the attenuation model, the velocity value in the crustal layer is not allowed to change in the inversion, because the phase velocity maps are corrected at all periods for the crustal effects calculated from the CRUST5.1 model (Mooney *et al.* 1998). These corrected maps, as a function of period, are then inverted to obtain the 3-D *S*-velocity model.

The *a priori* covariance of the attenuation model is described by *a priori* standard deviations as a function of depth. In order to allow larger Q_s variation in the lithosphere, which is believed to be more heterogeneous than the asthenosphere, a standard deviation on the *a priori* model σ_m was chosen to be twice as large in the lithosphere as in the asthenosphere (Billien 1999).

2.1.3 Resolution of the V_s and Q_s models

The problem of the effects of focusing/defocusing (as a result of refraction at strong velocity heterogeneities) on the wave amplitude was resolved by Billien (1999) by performing simultaneously a global inversion of the two seismic parameters, V_s and Q_s: it ensured full compatibility between the final V_s and Q_s models in terms of focusing/defocusing effects. Specifically, a linear approximation (Woodhouse & Wong 1986) was used to include the focusing effect in the inversion.

The observed attenuation is a mixture of scattering (largely as a result of reflection at velocity heterogeneities) and intrinsic (anelastic) attenuation. Because both of them lead to an exponential decay of amplitude with time (or epicentral distance; Billien 1999), they cannot be separated by inversion and a contribution of scattering into the observed attenuation cannot be completely ruled out even in the frequency range used in this study (Billien 1999).

In the regionalization, smooth models were favoured over rough models. This is achieved by use of a cost function based on the norm of the Lagrangian (second derivatives) of the model (Billien *et al.* 2000) rather than a classical damped least-squares method based on the norm of the model (e.g. Tarantola & Valette 1982). In our model, phase velocity and attenuation maps, and then V_s and Q_s maps, are represented by spherical harmonics up to degree $l = 20$. However, the effective degree of the computed maps is only 12 to 13, as a result of the damping used in the regionalization that progressively shuts off the highest degree terms. This effective degree corresponds to an *ca* 3000 km wavelength of attenuation and velocity lateral variations.

The vertical resolution of V_s and Q_s models is *ca* 50 km. The depth resolution matrix shows that the best resolved layer for Q_s is at a depth of 100 ± 25 km. Because Billien (1999) and Billien *et al.* (2000) use a damped inversion, the amplitude of Q_s variations at each depth layer within the lithosphere is probably underestimated. The tuning of the cost function in the first step of the inversion largely influences the absolute values of the Q_R variations (Billien *et al.* 2000) and thus the values of Q_s, but the sign of the variations and the sharpness of the contrasts are less sensitive to this tuning.

Both attenuation and velocity anomalies are calculated with respect to PREM (Figs 2–4), which was used as a reference model in the seismic inversion, because both V_s and Q_s models are global. Usage of PREM does not have a strong effect on calculated Q_s because focusing/defocusing effects depend not on absolute velocity values, but on the velocity gradient (Billien 1999). If a continent-dominated reference model were used in the seismic inversion, it would have led to a systematic shift of the absolute values, but would not have affected the general pattern of the anomalies. The difference in V_s between PREM and a preferable continent-dominated model is *ca* 2–2.5 per cent at the depth 100–150 km (Ritsema, private communication, 2003). The ocean-dominated PREM model led to a systematic shift to higher V_s on the continents, as can be clearly seen in Figs 2(a), 3(a) and 4(a), where white near-zero-anomaly regions correspond, in fact, to 0 to +3 per cent velocity anomalies. Because we are primarily interested in the patterns of velocity and attenuation variations and their correlations with temperature anomalies, the baseline of the reference model is not important for the further analysis.

2.2 Calculation of lithospheric temperatures

2.2.1 The model

The thermal state of the continental lithosphere has been addressed in numerous publications (see Artemieva & Mooney 2001, for references). However, most of these are regional studies and a lack of consistent assumptions on crustal heat production and thermal conductivity makes it impossible to combine them into a global model.

Two global studies of the thermal regime of the continental lithosphere are available at present. The model of Pollack & Chapman (1977) is based on a degree-12 spherical harmonic representation of global surface heat flow and provides an estimate of typical continental and oceanic geotherms and a rather generalized global map of lithospheric thermal thickness. In that model, continental geotherms were calculated assuming that 40 per cent of the mean surface heat flow arises from a near-surface, enriched radiogenic zone with a uniform 8 km thickness. Subsequent regional thermal and xenolith studies have proved that, on the whole, the set of geotherms calculated by Pollack & Chapman (1977) provides a good approximation of lithospheric temperatures. However, in some cratonic regions the assumptions behind this global model are invalid (e.g. Jaupart & Mareschal 1999).

Because cratons are expected to produce the strongest negative temperature anomalies within the continental lithosphere, here we use a more recent global thermal model for stable continents (Artemieva & Mooney 2001), in which regional seismic data on the crustal structure together with regional geological, petrological and laboratory data were used to constrain the vertical distribution of crustal heat production in different terranes (with sizes varying from approximately $1^\circ \times 1^\circ$ to $5^\circ \times 5^\circ$) and its total contribution to the surface heat flow. Models of the lateral and vertical distribution of heat production and thermal conductivity in the continental lithosphere used to constrain the thermal model are discussed in detail in Artemieva & Mooney (2001) and we refer the reader to the original publication for a detailed description of the data, the method and the calculation scheme. The consistency of assumptions for the depth distributions of thermal parameters in the thermal model permits the quantitative comparison of lithospheric geotherms, even if the calculated values contain systematic biases.

Estimates of the thermal regime of the stable continental lithosphere are based on the solution of the steady-state thermal conductivity equation, which allows the calculation of temperatures $T(z)$ within the crust and lithospheric mantle, constrained by borehole

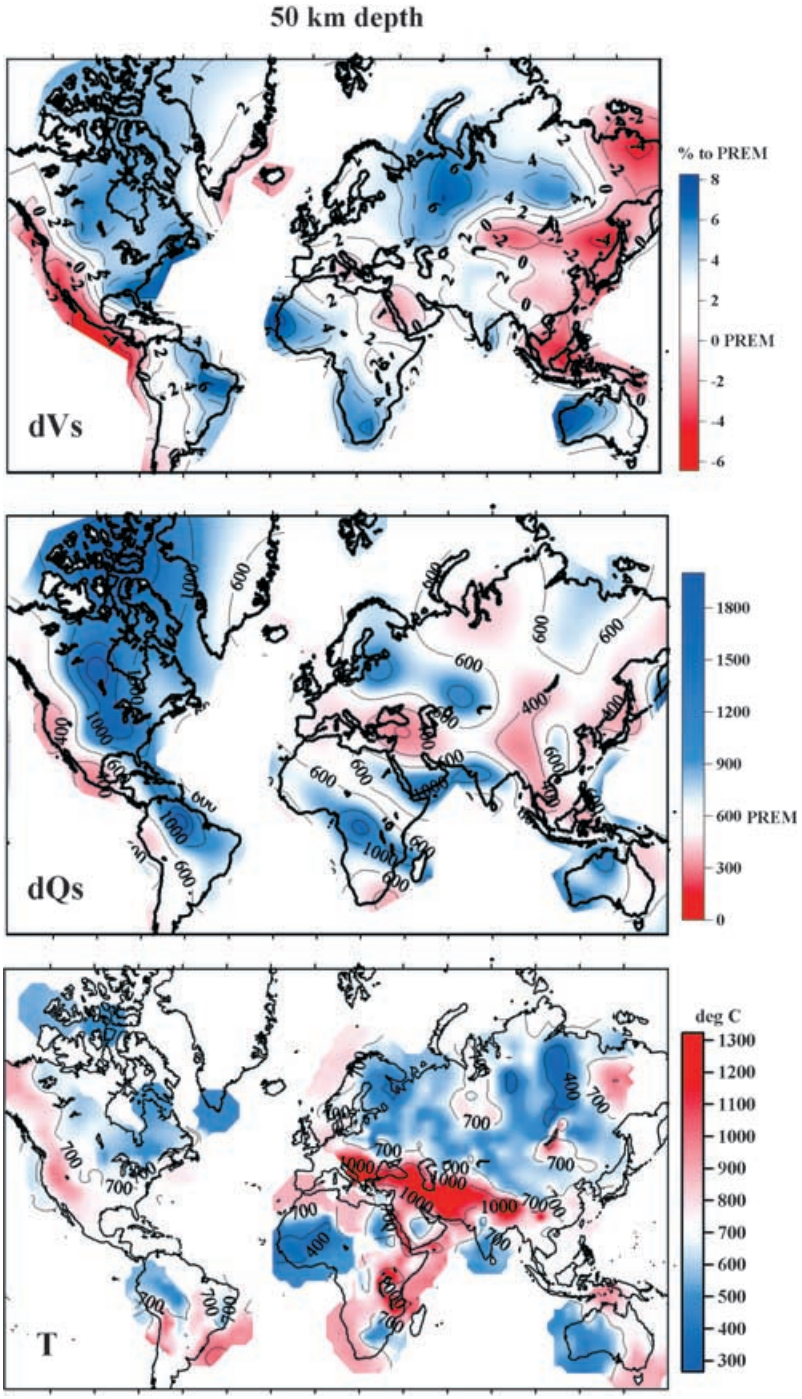

Figure 2. Map of shear wave velocity V_s (as variation in per cent relative to PREM), inverse attenuation Q_s, and temperature T (in °C) for continental lithosphere at a depth of 50 ± 25 km. Note that for the Tibetan plateau and the Andes, where the crustal thickness exceeds 60–70 km, the anomalies refer to the crustal depth, rather than to the subcrustal lithosphere. Blue colors correspond to cold regions with high V_s, high Q_s and low T. Red colors correspond to hot lithosphere with low V_s, low Q_s and high T. The dominant pattern on all three maps is the correlation of blue colors with stable Precambrian cratons and red colors with tectonically active Phanerozoic regions. The maps show a correlation in blue regions in the Canadian, Baltic, Siberian, West African and Australian cratons. Red regions that correlate include western North America, Europe, the Middle East, eastern China and eastern Australia.

heat flow measurements and the distribution of thermal parameters with depth. The global heat flow database (Pollack *et al.* 1993) updated for heat flow measurements reported since 1993 formed the basis for calculations of temperatures in the continental upper mantle. The lack of complete information on vertical and lateral distribution of crustal heat production (which is one of the key parameters controlling the resultant thermal models of the lithosphere), as well as the very uneven distribution of heat flow borehole data do not justify a 2-D or 3-D thermal modelling on a global scale. Errors associated with high lateral heat conduction can be large only in

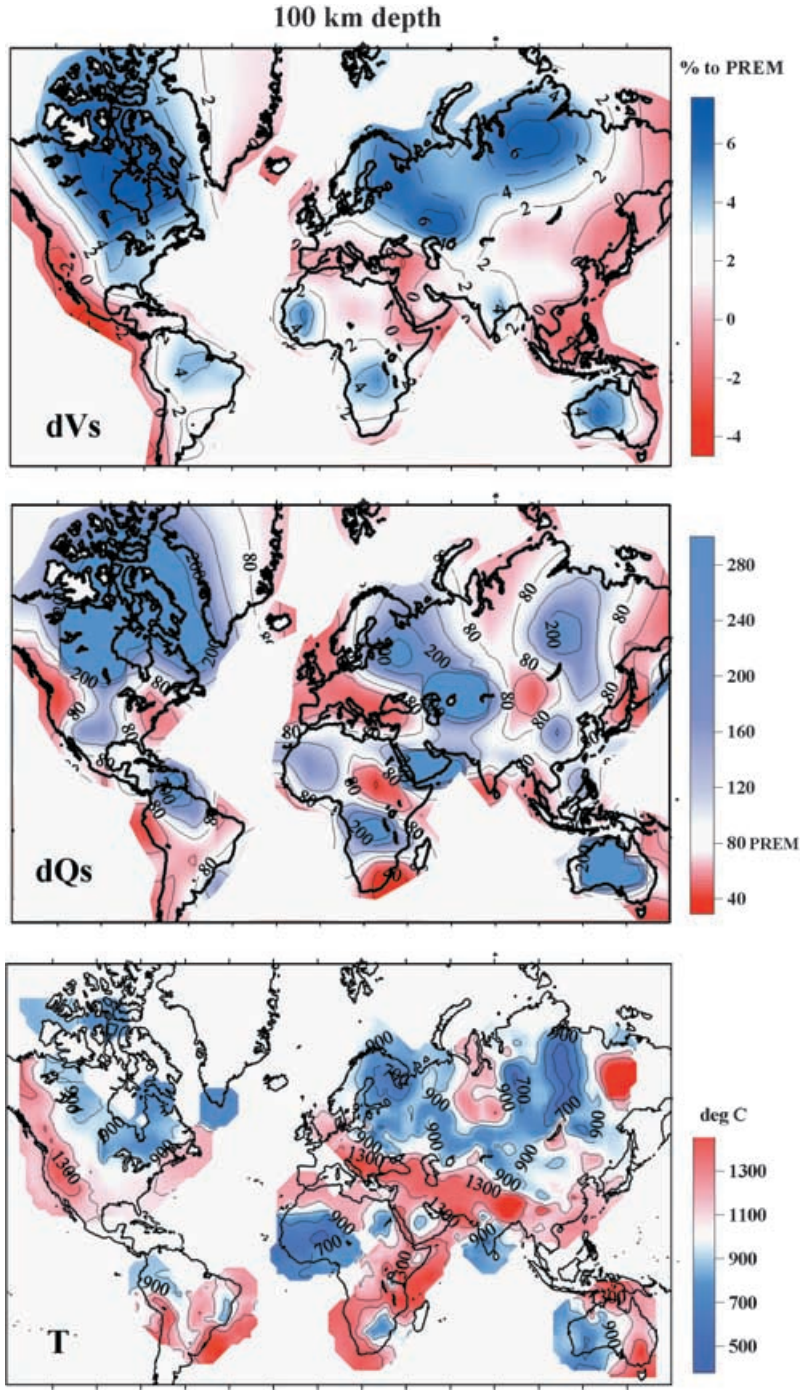

Figure 3. Map of shear wave velocity V_s (as variation in per cent relative to PREM), inverse attenuation Q_s and temperature T (in °C) for continental lithosphere at a depth of 100 ± 25 km. Presentation as in Fig. 2. There is a close correspondence in the anomaly patterns for most of the Precambrian cratons and the Cenozoic regions, especially for the Precambrian Eurasia, West Africa, northern Canada, western North America and central Australia. This correspondence indicates that temperature plays an important role in determining the strength of V_s and Q_s anomalies at this depth in the lithosphere.

regions with a strong contrast in heat production and/or conductivity (Jaupart 1983). However, assigning unconstrained values of thermal parameters and surface heat flow in areas with scarce or non-existing data would have introduced uncontrolled errors into the entire model.

The estimates of the lithospheric thermal thickness are in a good agreement with global and regional seismic tomography results, and with regional xenolith geotherms (*cf.* Artemieva & Mooney 2001). The maps of temperature distribution in the continental lithosphere at the depths of 50, 100 and 150 km form the basis of our comparison

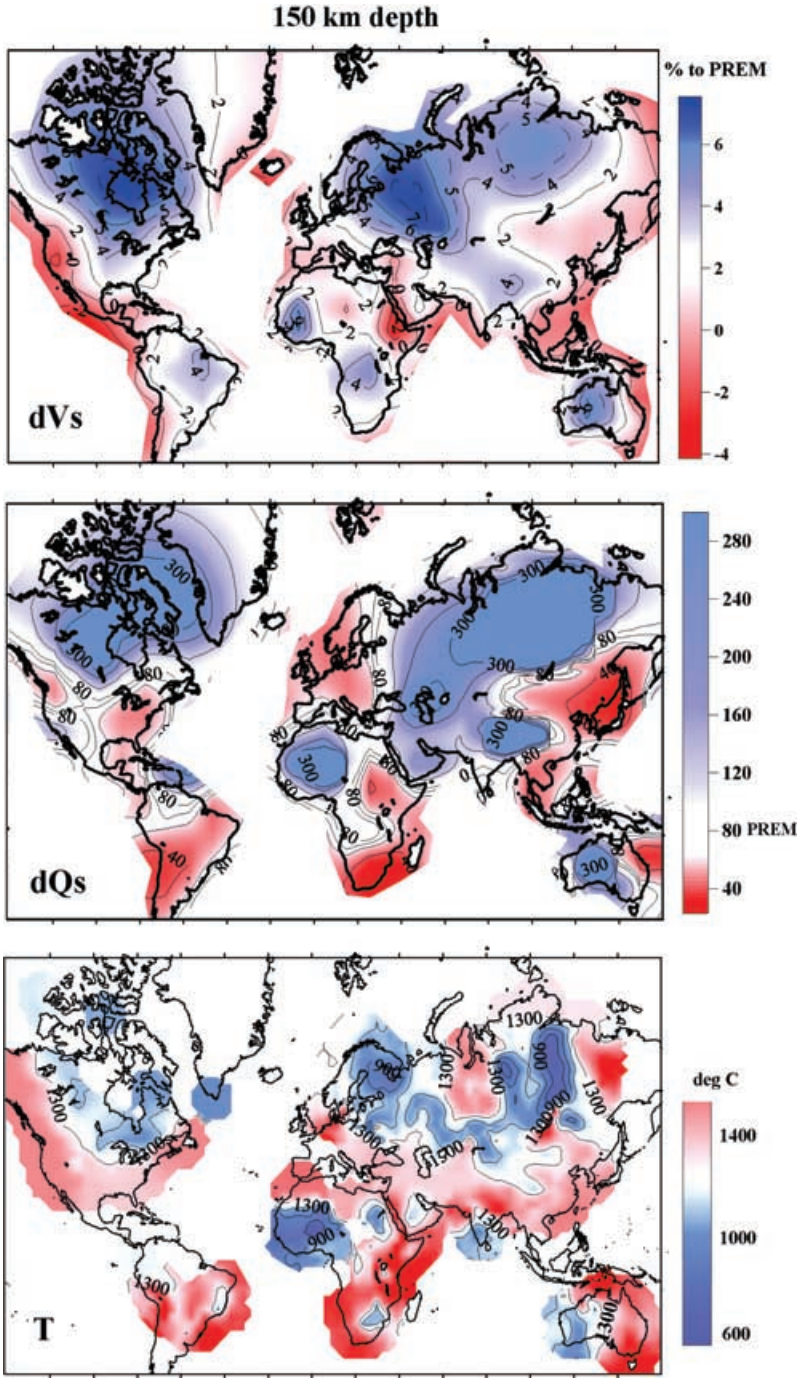

Figure 4. Map of shear wave velocity V_s (as variation in per cent relative to PREM), inverse attenuation Q_s and temperature T (in °C) for continental lithosphere at a depth of 150 ± 25 km. Presentation as in Fig. 2. All low temperatures (lower panel) correspond to stable cratons. In contrast, high V_s and high Q_s anomalies include these same stable cratons plus some regions of active tectonics, such as the southern Eurasia suture zone extending from the Alps to the Tibetan plateau. This may indicate the presence of cold subducted lithosphere beneath the southern European suture zone. High mantle temperatures (>1300 °C, shown by red colors in Fig. 4c) dominate the non-cratonic parts of the continents and imply a lithospheric thickness less than 150 km, if defined as the conductive layer above the mantle adiabat of 1300 °C.

of lateral variations of temperature, V_s and Q_s at different depths in the continental lithosphere.

2.2.2 *Resolution of the T models*

The constraints provided by the thermal model are reliable for stable continental regions, where the assumption of a steady-state thermal regime of the lithosphere is valid. For most tectonically active regions (e.g. the Alpine–Himalayas region, the Andes and western USA) the temperature distribution in the upper mantle is not calculated from surface heat flow but is based on available petrologic and non-steady-state constraints (e.g. Lachenbruch & Sass 1977; Polyakov *et al.* 1988; Henry *et al.* 1997; Le Pichon *et al.* 1997). Lithospheric temperature maps are calculated from point (i.e. borehole) data (for heat flow data coverage see Fig. 5) and give

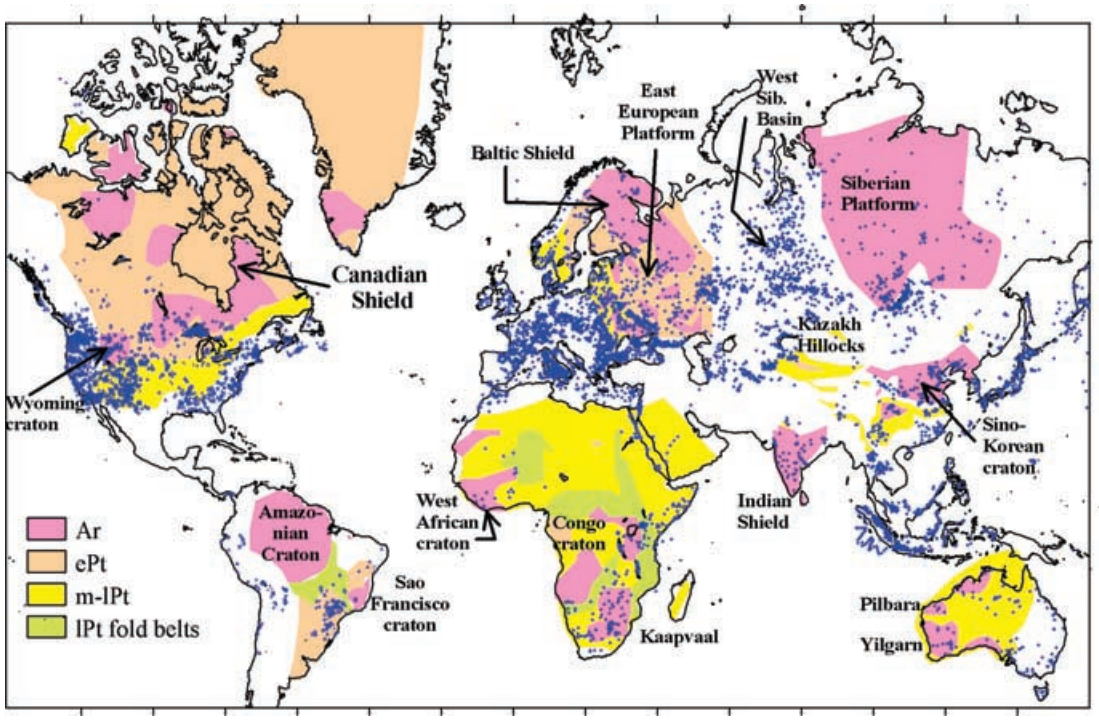

Figure 5. Location of Precambrian cratons and sites of borehole heat flow measurements on the continents [based on global heat flow compilation (Pollack *et al.* 1993) updated for heat flow measurements reported in 1993–1999].

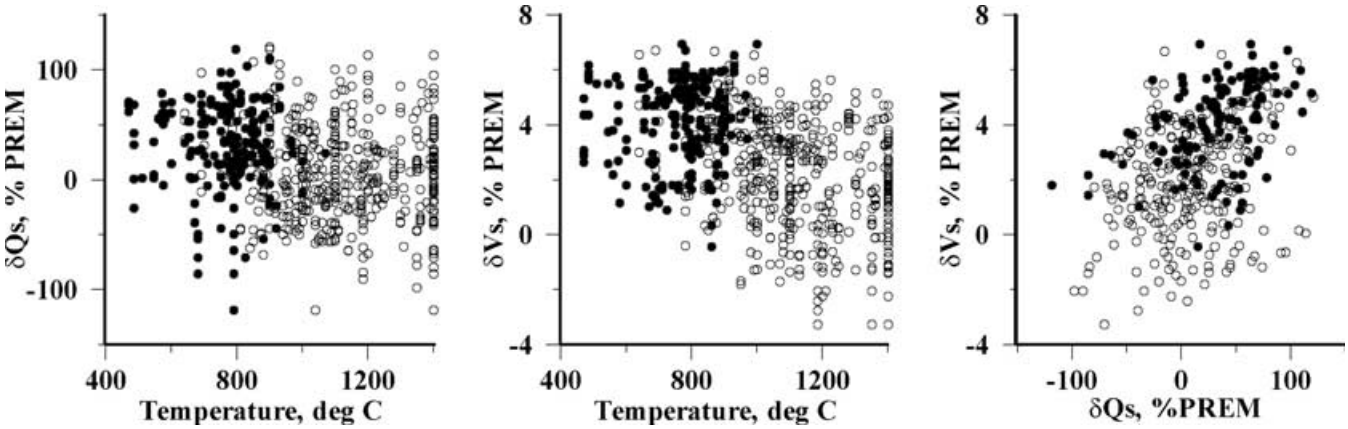

Figure 6. Correlations between shear wave velocity V_s (as variation in per cent relative to PREM), inverse attenuation Q_s (as variation in per cent relative to PREM) and temperature T (in °C) for continental lithosphere at a depth of 100 km. V_s and Q_s values are for the sites of thermal modelling. All data for the continents (open circles); data for Archean and early Proterozoic cratons only (solid circles). The calculated correlation coefficients are less than 0.42 for any pair of the parameters (see Table 1). The correlation is especially bad for the Archean–early-Proterozoic cratons, suggesting that a significant part of lateral V_s and Q_s variations in cratonic lithosphere has a non-thermal origin.

estimates of $T(z)$ in the lower lithosphere with an accuracy of *ca* 100°C (see Artemieva & Mooney 2001, for sensitivity estimates). These local geotherms calculated for regions with typical sizes of 1° × 1° to 5° × 5° were interpolated by krigging with an interpolation radius of 10° (Figs 2c, 3c and 4c) that preserved the accuracy of $T(z)$ estimates in the vicinity of heat flow boreholes and provided smoothed anomaly contours between them.

Note that interpolation of local geotherms introduces artefacts in the form of unconstrained haloes in regions with scarce borehole data (e.g. the Arabian shield, Central Africa, South America, northern Canada and Greenland) that can extend as far as 1000 km from sites of heat flow measurements. In regions with a strong contrast in tectonic and thermal regimes (e.g. the transition between stable continental USA and western North America, or the transition between Precambrian and Variscan Europe, or East African rift system), an interpolation resulted in a smeared thermal contrast. Thus, the spatial resolution of the temperature maps is uneven, but is within a range of 200–1000 km and is significantly higher than the lateral resolution of seismic attenuation and shear wave velocity maps.

Table 1. Correlation coefficients between seismic velocity, attenuation, temperature and surface heat flow at different depths in the continental upper mantle.

Parameters	$z = 50$ km	$z = 100$ km	$z = 150$ km
Q_s vs. T (*)	−0.22	−0.33	−0.47
ln Q_s vs. $1/T$ (*)	0.27	0.31	0.36
V_s vs. T (*)	−0.31	−0.56	−0.56
V_s vs. Q_s (*)	0.38	0.66	0.41
Q_s vs. surface heat flow (*)	−0.19	−0.18	−0.04
V_s vs. surface heat flow (*)	−0.26	−0.39	−0.36
Q_s vs. T (black and white)	−0.24	−0.24	−0.25
V_s vs. T (black and white)	−0.20	−0.36	−0.26
V_s vs. Q_s (black and white)	0.23	0.48	0.28
Q_s vs. T (all data)	−0.19	−0.23	−0.34
V_s vs. T (all data)	−0.19	−0.38	−0.42
V_s vs. Q_s (all data)	0.38	0.41	0.41

(*) At each depth, values within the band around the average value (zero anomaly), approximately corresponding to white areas in Figs 2–4, are excluded from the analysis. The width of the band is 10 per cent of the total range of parameter variations. The correlations for $V_s - Q_s$ and $Q_s - T$ at $z = 50$ and 150 km and for $V_s - T$ at $z = 50$ km should be treated with caution as a result of low resolution of V_s and Q_s models at these depths. For a comparison, we calculated the correlation between the signs of the anomalies only (black and white models) and excluding the 10-per-cent-wide band around the average value from the statistical analysis. Lower correlations indicate that the amplitudes of the anomalies are important in global correlations. Correlation coefficients calculated when all data were included into the analysis are presented for a comparison as well.

3 QUANTITATIVE CORRELATIONS V_s–Q_s–T

3.1 Calculation of correlation coefficients

Laboratory evidence for a strong correlation between seismic parameters and temperatures has recently been used in a number of studies to constrain mantle temperatures from elastic and anelastic tomography (e.g. Sobolev *et al.* 1996; Sato *et al.* 1988). We next discuss a validity of these approaches and examine the quantitative correlation between each pair of the parameters V_s, Q_s and T at depths 50, 100 and 150 km (Table 1). To calculate the correlation coefficients (r), seismic data were converted from spherical harmonic representation to a $1^\circ \times 1^\circ$ spatial grid. Two interpolations of temperatures were calculated from local geotherms: (i) with a 5° radius to reduce artefacts of interpolation in regions with sparse data and (ii) with a 30° radius to bring the temperature model to a resolution comparable to the resolution of seismic models. These interpolated temperature maps were resampled to a $1^\circ \times 1^\circ$ spatial grid. In the case of a 30° interpolation, correlation coefficients between seismic parameters and T are *ca* 0.05 weaker than in case of a 5° interpolation, probably as a result of interpolation haloes unconstrained by heat flow data: thus, we further discuss only the results for a 5° interpolation of mantle geotherms.

Correlations between the parameters V_s, Q_s and T were calculated on a $1^\circ \times 1^\circ$ grid: for each of the parameters the values were normalized by the maximum amplitude calculated for each depth. We first included all V_s, Q_s and T data into the analysis. The correlation coefficients were very low, less than 0.42 for any pair of the parameters and at any depth and, when plotted as x–y plots, formed clouds (Fig. 6). Roth *et al.* (2000) found similar clouds when comparing global attenuation and velocity models [QR19 of Romanowicz (1995) and S12_WM13 of Su *et al.* (1994)]. The correlation is in particular low for the Archean-early Proterozoic cratons, suggesting that for these regions a significant part of lateral V_s and Q_s variations has a non-thermal origin. Because the correlation coefficient is sensitive to the sign of seismic and temperature anomalies when their amplitudes are small, we next excluded from the correlation analysis the bands around the zero-value anomalies. The width of the bands was chosen as 10 per cent of the total range of parameter variations around the average value (zero anomaly): it approximately corresponds to the white areas in Figs 2–4 and is close to uncertainties in amplitudes in seismic and temperature models.

3.2 V_s–T correlation

Strong effect of temperature on seismic velocities is well-known from laboratory studies (Fig. 1). However, our statistical analysis of the V_s–T correlation in the upper mantle of the continents suggests that even though there is the expected negative correlation between the two parameters ($r = -0.56$ at $z = 100$ and 150 km; Table 1), the conversion of seismic velocities into temperatures (e.g. Sobolev *et al.* 1996; Goes *et al.* 2000; Goes & van der Lee 2002) is subject to considerable uncertainty. Our data show that at a depth of 100 km, the range of possible temperatures corresponding to any given velocity value is at least ± 250 °C (Fig. 6). This indicates that a significant part of the velocity anomalies in the continental upper mantle can be the result of physical mechanisms other than thermal (i.e. compositional heterogeneities, anisotropy, fluids, or melts). With the present resolution of seismic and thermal models it is, however, difficult to say which part of the V_s variations has a true non-thermal origin. We further address this question in Section 5.3. Here we note that the maximum values of V_s anomalies are found for the Canadian shield and the East European and Siberian cratons. Although recent studies suggest that the temperature effect on velocities is much stronger than iron content variations (Deschamps *et al.* 2002), compositional difference between the Precambrian and Phanerozoic subcrustal lithosphere (e.g. Boyd 1989; Griffin *et al.* 1999) can be partly responsible for low V_s–T global correlation on the continents.

3.3 Q_s–T correlation

An exponential law for the correlation of temperature and seismic attenuation has long been known from laboratory experiments (Fig. 1). Sato *et al.* (1988) were among the first to apply it to constrain oceanic geotherms from seismic attenuation and laboratory data. Other attempts to calculate temperatures from seismic attenuation data include studies by Sarker & Abers (1999) for the crust of south-central Eurasia and by Nakajima & Hasegawa (2003) for the mantle wedge beneath northeastern Japan. Though seismic data show the existence of a regional correlation between deep temperatures and attenuation (e.g. Bodri *et al.* 1991), the statistical analysis (Table 1) shows that, globally, the correlation coefficient peaks at $r = -0.47$ at $z = 150$ km and is much weaker at shallower depths (e.g. $r \sim -0.33$ at $z = 100$ km, where the resolution of the attenuation model is the best). Because experimental studies suggest a logarithmic dependence of Q_s on T (eq. 1), we have also calculated the correlation coefficient between $\ln(Q_s)$ and $1/T$ and found it to be very close to the Q_s–T correlation. A poor global correlation between Q_s and T on the continents (less than 0.47 at any depth, regardless of the way it has been calculated) suggests that, as for V_s, effects other than temperature (e.g. composition, fluids, partial melt) play an important role in producing attenuation anomalies in the upper mantle.

In stable continental regions, where a presence of partial melts or fluids at a 100 km depth is unlikely, one would expect that

compositional variations could play the dominant role in smearing the correlation between Q_s and T. However, no experimental studies have examined how depletion can influence seismic attenuation. Recent laboratory measurements of attenuation in MgO (Getting *et al.* 1997) suggest that a difference in Mg content in the subcrustal lithosphere of the cratons and Palaeozoic platforms can be reflected in Q_s values. Because cratonic lithosphere was formed by a collage of continental and oceanic terranes with different structure and bulk composition, large-scale lithospheric heterogeneities can produce scattering and also be responsible for a lack of Q_s–T correlation. A regional study of the Japan islands has demonstrated that scattering can account for 10–30 per cent of the measured attenuation (Hoshiba 1993). Nevertheless, if variations of scattering in the upper mantle are small, the correlation between intrinsic (and total) attenuation and temperature will still hold.

3.4 Q_s–V_s correlation

Because laboratory measurements on olivine-rich rocks suggest that both velocity and attenuation are strongly temperature dependent, one may expect V_s and Q_s to be correlated, as indicated by regional (e.g. Sheehan & Solomon 1992; Tsumura *et al.* 2000) and global studies (Romanowicz 1995). For example, for the Fiji–Tonga region, Roth *et al.* (2000) found that, at depths greater than 100 km, both anomalies are strongly correlated and can be fit by an exponential equation; at shallower depths their data show a high degree of scatter. They also examined the correlation between V_s and Q_s anomalies derived from global seismic tomography studies (Su *et al.* 1994; Romanowicz 1995) and concluded that the strong correlation between the two parameters in the Tonga subduction zone is more a regional phenomenon than a general rule. The statistical analysis of a global Q_s–V_s data set for the continents presented here (Table 1) supports this conclusion. At 100 km depth we observe the correlation $r = 0.66$ between Q_s and V_s in the upper mantle of the continents: this is the highest correlation we found for any pair of the parameters. Higher sensitivity of Q_s than V_s to temperature variations (e.g. Berckhemer *et al.* 1982; Karato & Spetzler 1990; Jackson *et al.* 1992) can be partly responsible for the moderate global correlation between Q_s and V_s.

3.5 Why are correlation coefficients so low?

Low correlation coefficients between V_s, Q_s and T determined in statistical analysis for the continents contradict laboratory data on a strong dependence of V_s and Q_s on T. However, our correlation coefficients for 100 km depth (where high resolution is expected for both V_s and Q_s models) are significantly higher ($r = -0.56$ and -0.33, correspondingly) than found for a global correlation between the QR19 attenuation model and surface heat flow ($r = 0.20$–0.35) at $z < 250$ km (Romanowicz 1995). On the other hand, when the oceanic upper mantle is excluded from the analysis, the correlation between Q_s model and surface heat flow becomes weaker ($r \sim -0.20$) (Table 1).

Relatively weak global correlations between thermal and seismic anomalies in the continental upper mantle suggest that, globally, temperatures alone cannot explain a large part of attenuation and velocity variations. A set of different physical mechanisms as well as artefacts associated with inversion, resolution and interpolation can deteriorate the global V_s–Q_s–T correlations from what can be expected from experimental studies.

(i) Accuracy of seismic and thermal models used in this study:

(a) Attenuation measured in laboratory includes only anelastic attenuation (eq. 1). However, the attenuation model used in the present study also includes scattering effects, which could not have been separated during the inversion.

(b) Uncertainties in V_s and Q_s models can further affect calculated correlation coefficients. In some regions, strong offshore seismic anomalies are smeared into onshore regions.

(c) Errors in temperature estimates can be high in tectonically active regions, where temperature constraints from data on regional metamorphism were extrapolated to mantle depths.

(d) Seismic models provide a snap-shot of the physical state of the upper mantle, while surface heat flow reflects its past thermal regime. In some regions this can produce apparently non-correlated seismic and thermal anomalies.

(e) Seismic and thermal models have different lateral resolution and different spatial coverage. Because Q_s and V_s models were calculated in simultaneous inversion from the same seismic data set and have the same lateral resolution, one would expect a strong Q_s–V_s correlation, if Q_s and V_s were not affected by thermal, compositional and fluid regime variations in a different way. Thus, low correlation coefficients can hardly be attributed solely to resolution problems and uncertainties in seismic and thermal models and raise the possibility that non-thermal effects on V_s and Q_s are significantly larger than usually assumed.

(ii) Anisotropy: The effect of anisotropy on surface waves at the periods used in the present study was examined recently by Trampert & Woodhouse (2003). However, our seismic models do not account for azimuthal anisotropy in the upper mantle. This oversimplification may introduce biases in seismic models. Such biases are generally small and their effects on the velocity and attenuation contrasts are likely to be even smaller, and thus should not significantly affect V_s–Q_s–T correlations.

(iii) Variations in composition and mineralogy: The effect of mantle composition and mineralogy on V_s has been previously studied in detail (e.g. Nolet & Zielhuis 1994; Jackson & Rigden 1998; Goes *et al.* 2000; Deschamps *et al.* 2002). Based on forward calculations, these authors conclude that variations of iron content in the lithospheric mantle have a larger effect on V_s than any other variations in composition and mineralogy. However, their effect is significantly smaller than the effect of T variations: for example, a 1 per cent V_s anomaly can be explained either by a 4 per cent variation of iron content or by a thermal anomaly of 50–100 °C (Nolet & Zielhuis 1994; Deschamps *et al.* 2002). Little is known of the effect of MgO or FeO variations on the attenuation (Getting *et al.* 1997). However, the results of Billien *et al.* (2000) and Sarker & Abers (1998) show a systematic decrease of Q_s with tectonothermal age of continental lithosphere. Thus, we cannot rule out the possibility that compositional variations in continental upper mantle can affect Q_s–T and V_s–Q_s correlations.

(iv) Partial melts and fluids: Stable continental lithosphere is drier compared with oceanic lithosphere (Hirth *et al.* 2000). Thus, in >100 km thick lithosphere of Palaeozoic and Precambrian platforms, one would not expect neither fluids nor partial melts to play an important role in velocity or attenuation anomalies in the upper 100 km. Except for special tectonic settings (e.g. Nolet & Zielhuis 1994), Q_s and V_s anomalies there are likely to be compositional. In tectonically active regions, even at near-solidus temperatures, the dependence of velocity and attenuation on temperature variations becomes strongly non-linear (e.g. Sato & Sacks 1989; Sato *et al.* 1989; Jackson *et al.* 1992). A small percentage partial melting dramatically affects shear modulus and shear wave attenuation through direct thermoelastic losses (Anderson 1989; Sato *et al.* 1989; Jackson *et al.* 1992; Karato 1993). Because the effect

of T on Q_s and V_s is different (a sharp increase in Q_s occurs at lower temperature than a drop in V_s associated with partial melting, Fig. 1), this can decrease global correlations between V_s, Q_s and T. Romanowicz (1995) argues that exponential dependence of attenuation on T favours hotter anomalies (even when cold anomalies have larger amplitude), while velocity is more sensitive to cold anomalies as a result of its linear dependence on T. A presence of volatiles or fluids associated with subduction zones (Carlson & Miller 2003) can significantly lower the solidus and thus have a strong effect on Q_s and V_s. Thus, we conclude that the local presence of partial melts and/or fluids may weaken global V_s–Q_s–T correlations.

Because we are unable to separate the effects of the lack of resolution in our data from true non-thermal effects, we next examine regional qualitative correlations between V_s, Q_s and T (Section 4) to test if, regardless of low global correlation values, temperature plays a governing role in producing regional seismic anomalies. We further use theoretical and laboratory data to quantify which part of observed variations in seismic attenuation and shear wave velocities can be predicted from thermal anomalies alone (Section 5).

4 QUALITATIVE COMPARISON OF V_s, Q_s AND T ANOMALIES IN THE UPPER MANTLE

4.1 General remarks

We visually compare maps (Figs 2–4) of seismic and temperature anomalies in the upper mantle to examine if there is a qualitative regional correlation between the parameters. Because at 50 km depth the crustal structure has the largest influence on the V_s and Q_s values, we place greater emphasis on the maps for 100 and 150 km depth, with particular focus on the results for 100 km depth, where the resolution of both of the seismic models is the highest. For a typical continental geotherm (corresponding to surface heat flow of *ca* 60 mW m^{-2}), lithospheric temperatures at 100 km depth are close to 1000 °C. At seismic frequencies, a strong solid-state viscoelastic relaxation expressed as a sharp increase in seismic attenuation is expected in the upper-mantle crystalline rocks at high homologous temperatures (e.g. Berckhemer *et al.* 1982). This means that anelastic anomalies of thermal origin should be best correlated with temperature at a depth of 100 km. Indeed, white areas with a near-zero Q_s anomaly generally correlate with a 1000–1100 °C isotherm (Fig. 3).

A comparison of the three maps presented in Figs 2–4 reveals the existence of a strong overall qualitative correlation between the signs of V_s, Q_s and T anomalies for most of the continental lithosphere at depths of 50–150 km. At first look, there is less correlation between the three maps for a depth of 150 km. The eye catches strong positive seismic anomalies over North America and Eurasia, where temperature anomalies appear to be much weaker. Nevertheless, the maps reveal a good qualitative correlation between the signs of the anomalies at this depth as well.

4.2 Regions where all three parameters correlate

There are two types of regions where all three anomalies correlate: cold regions, which include most of the Precambrian cratons, and hot regions such as continental rifts, Cenozoic orogens and, unexpectedly, the Sino-Korean craton. The signs of all three anomalies correlate within both of the groups throughout the entire lithosphere, which suggests a primarily thermal origin of most of the seismic anomalies.

Hot (red) anomalies (low V_s, low Q_s and high T) are found in all three maps (Figs 2–4) in most tectonically active regions of the continents. At all depths, blue, cold anomalies with high V_s, high Q_s and low T dominate in cratonic regions (see Fig. 5 for a location map). For example, high V_s, high Q_s and low T are seen beneath the West African craton and the western-central part of Australia, in agreement with recent regional shear wave tomography studies (Simons *et al.* 1999; Debayle & Kennett 2000).

On the whole, we find a better agreement between T and Q_s for large cratons (the Canadian shield, the Baltic shield, the East European platform and the Siberian craton) than for small ones. For example, a strong correlation between all three anomalies (V_s, Q_s and T) is observed at 100 km depth beneath most of Eurasia, with the strongest anomalies beneath the East European and the Siberian cratons separated by a hot high-temperature and high-attenuation anomaly beneath the Palaeozoic West Siberian basin (WSB). However, at 150 km depth, pronounced low attenuation in the WSB (Figs 4b and 7c) does not correlate with high temperature (Fig. 4c).

In the Canadian shield, the magnitude of the T anomaly is significantly weaker than the magnitude of the Q_s and V_s anomalies, probably because all borehole heat flow data are located at the periphery of the Canadian shield. The values of the temperature anomalies in our model (Fig. 3c) are close to the estimates of Goes & van der Lee (2002), who calculated lithospheric temperature in North America from seismic tomography data, assuming that V_s anomalies are caused by temperature variations. The good agreement between two independent estimates of lithospheric temperatures beneath stable North America indicates that shear wave velocity anomalies in the Precambrian lithosphere are indeed chiefly of thermal origin.

The Early Proterozoic Sino-Korean craton shows near-zero anomalies in the three maps at 100 km depth and hot anomalies in the maps for 150 km. Surface wave tomography (Huang *et al.* 2003), heat flow data (Artemieva & Mooney 2001) and studies of mantle xenoliths (Xu *et al.* 2000) indicate an atypically thin (120–150 km) Sino-Korean lithosphere compared with other Precambrian cratons. Furthermore, the lower part (below 80–140 km depth) of the cratonic lithosphere could have been largely replaced by more fertile Phanerozoic material (Griffin *et al.* 1998). Thus, part of the V_s and Q_s variations there may probably have a non-thermal origin (possibly including compositional variations at *ca* 100 km depth and partial melting below *ca* 150 km depth).

4.3 Regions where only seismic anomalies (V_s and Q_s) correlate

Of particular interest are the regions where the seismic anomalies V_s and Q_s have the same sign, but do not correlate with temperature anomalies, because such pattern can be indicative of a clearly non-thermal origin of the seismic anomalies. The East African rift zone is one of the regions that exhibits such non-correlated behaviour of seismic and thermal anomalies. However, this rift is too narrow to be reliably resolved by seismic models used in the present study. The Tibet–Himalayan orogen is consistently evident only in the map of T. However, temperature estimates for this tectonically active region based on regional metamorphism data should be interpreted with caution. A large time delay in the upward propagation of a thermal anomaly also implies that the correlation between seismic and thermal models should be best in stable regions that did not undergo tectonic or magmatic activity over a long geological time. Thus, we cannot identify any region where seismic anomalies are clearly of a non-thermal origin.

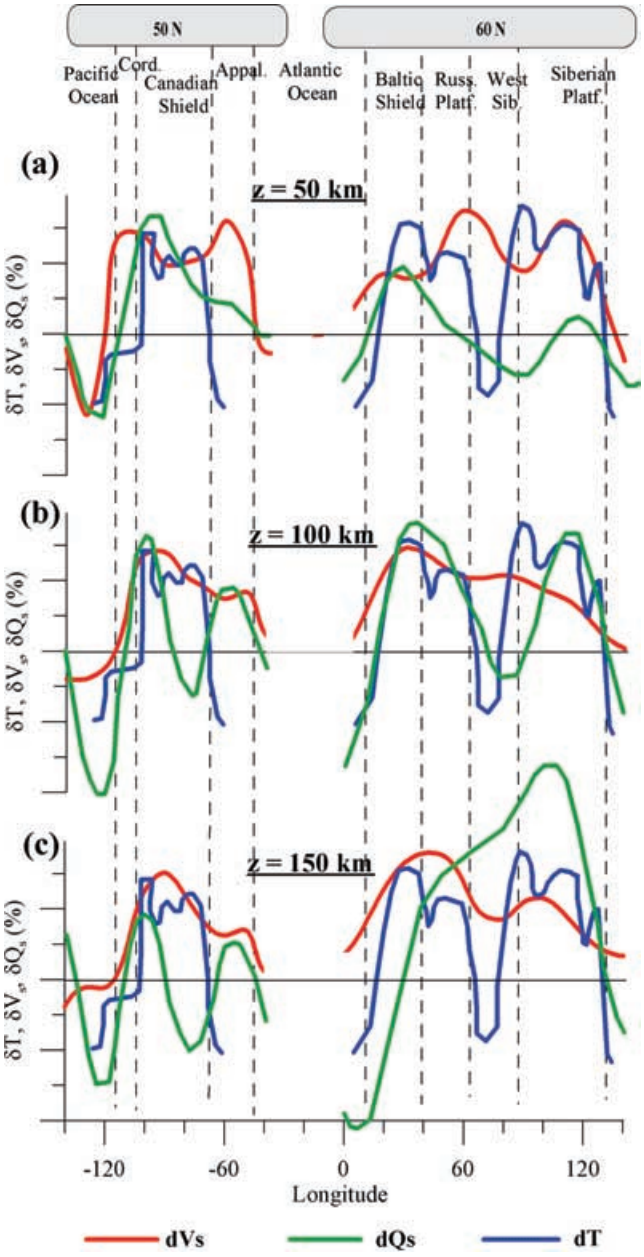

Figure 7. Comparison of Q_s, V_s and T at a depths of 50, 100 and 150 km along the latitude 50°N in North America and the latitude 60°N in Eurasia. The values of V_s, Q_s and T are averaged over a 10° band, centered correspondingly on 50°N or on 60°N. Large ticks on the y-axis correspond to the 4 per cent anomaly for V_s, 40 per cent anomaly for Q_s and −20 per cent anomaly for T. Q_s and V_s anomalies are shown as variation with respect to PREM. T anomaly is shown with respect to a typical continental geotherm of 55–60 mW m^{-2} (i.e. *ca* 750, 1000 and 1250°C at three depths, correspondingly). An accuracy in the amplitudes of T model is *ca* 10 per cent, so that the signs of the anomalies are the robust features. The lateral resolution of thermal and seismic models is different (*ca* 20° for Q_s and V_s anomalies and *ca* 10° for T anomalies), such that their peaks may not necessarily coincide. The resolution of seismic data is the lowest at 50 km depth as a result of crustal effects. On the whole, there is a good general agreement between V_s and T anomalies. However, at 100 km depth where the resolution of the attenuation model is the highest, Q_s and T anomalies in Eurasia show an excellent agreement.

4.4 Regions where V_s and T anomalies do not correlate with Q_s

The regions with non-correlated seismic anomalies in the lithosphere (which include the SW Baltic shield and the South African craton) deserve special attention, as both V_s and Q_s anomalies used in this study were derived in a joint inversion of the same carefully selected data set (Billien 1999; Billien *et al.* 2000). According to experimental studies on polycrystalline olivine at seismic frequencies (e.g. Jackson 2000), attenuation in shallow lithosphere, however, needs not correlate with temperature and shear wave velocities, because at low T (< 600° C) the upper-mantle rocks exhibit an almost elastic behaviour, while the values of Q^{-1} are essentially scattered.

The late Proterozoic southwestern part of the Baltic shield is close to the transition zone from depleted Precambrian lithosphere to fertile, younger lithosphere. The transition (the Trans-European suture zone, TESZ) is marked by a sharp contrast in crustal structure, surface heat flow and lithospheric thickness. In maps for 50 and 100 km depths, the V_s, Q_s and T anomalies approximately follow the NW–SE orientation of TESZ. However, at 150 km depth the attenuation anomaly has a N–S orientation (Fig. 4b). This anomaly may imply the presence of partial melt and/or fluid inclusions in the metasomatized lithosphere, which at near-solidus temperatures would affect Q_s stronger than V_s (Mitchell 1995). This hypothesis is supported by electrical studies (Jones 1984, 1999), which imply a presence of a well-conducting asthenosphere at *ca* 160–190 km depth in the western part of the Baltic shield. Deep mantle reflections seen in the BABEL seismic profile in the same region give evidence for the Proterozoic subduction (BABEL Working Group 1990) and thus regional fluid enrichment of the lithosphere can be expected there. Part of the apparent anelastic attenuation anomalies in the Baltic shield may also be the result of scattering effects in the upper mantle that was reworked during the late Proterozoic tectonic activity in the region (e.g. Gaal & Gorbatschev 1987), when large volumes of rapakivi granitic intrusions were emplaced (Haapala & Rämö 1991), followed by Palaeozoic rifting (e.g. Neumann *et al.* 1995). As a result, the marginal part of the cratonic lithosphere could have been partly detached and/or metasomatized.

Surprisingly, southern Africa, including the Kaapvaal craton, does not show the expected high V_s anomaly typical for other cratons, while temperature estimates suggest that the lithosphere is cold (e.g. Jaupart & Mareschal 1999; Artemieva & Mooney 2001). Moreover, it has a strong mantle attenuation, and V_s and Q_s anomalies disagree there at all lithospheric depths. However, the discrepancy between the signs of the anomalies is likely to be a resolution artefact. The apparently highly attenuating region at 100 km depth beneath South Africa may partly result from smearing of a strong offshore anomaly (see the maps in Billien *et al.* 2000). Similar explanation of low V_s uncorrelated with low T applies to the Indian shield, where a strong offshore seismic anomaly is observed.

4.5 Regions where Q_s and T do not correlate with V_s

Regions where neither Q_s nor T anomalies correlate with V_s anomalies in the deep lithosphere ($z \sim$ 100–150 km) include the West Siberian Basin (WSB) and the Arabian shield. However, the lateral dimensions of the Arabian shield are too small to be resolved by the seismic models used in the present study and only a few heat flow measurements are available there. We favour a compositional origin of the velocity anomalies beneath the WSB, because laboratory and theoretical studies indicate that seismic velocities are more sensitive

to compositional variations than seismic attenuation (e.g. Bina & Silver 1997). We further address this question in Section 5.3.

4.6 Comparison of V_s, Q_s and T along a 50°N–60°N profile

A global profile at 50°N latitude in North America and at 60°N latitude in Eurasia permits the examination of regional correlations between V_s, Q_s and T in more detail, because the temperature model used in this study is well constrained only for stable continents. Thus, our choice of a profile has been dictated by a wish to compare V_s, Q_s and T primarily in platform regions that have good heat flow data coverage.

As discussed earlier, there is a good general agreement between V_s and T anomalies for the cratonic regions (the Canadian shield, the Russian (East European) platform and the Siberian platform). At 100 km depth (Fig. 7b) where the resolution of the attenuation model is the highest, Q_s and T anomalies in Eurasia show a perfect agreement. Increased attenuation at the southeastern margin of the Canadian shield observed at 100–150 km depth results from smearing of a high attenuation anomaly centered over the Appalachians (compare with Fig. 3b). As discussed in the previous section, the non-correlated behaviour of the anomalies in the WSB is likely to be caused by compositional variations. Thus, we conclude that, despite relatively low values of correlation coefficients, a significant part of seismic anomalies in stable continental lithosphere has a thermal origin.

5 COMPARISON OF SEISMICALLY MEASURED V_s AND Q_s AND THEORETICAL V_s^T AND Q_p^T

5.1 Calculation of theoretical Q_p^T in the upper mantle from T

With the available data set we were unable to confirm that, statistically, T is the dominant factor for Q_s and V_s variations on a global scale (Section 3). This appears to contradict numerous laboratory measurements that demonstrate the temperature dependence of seismic attenuation and provide the basis for estimates of attenuation in the upper mantle of a purely thermal origin, Q_p^T (eq. 1). Moreover, qualitative comparison shows that on the regional scale the signs of seismic and temperature anomalies in the continental lithosphere are correlated (section 4). Though the robust extrapolation of experimental data to seismic attenuation in the real Earth is controversial (e.g. Jackson 2000), a comparison of Q_p calculated from Q_s from global anelastic tomography with theoretical predictions for Q_p^T from temperatures would permit to distinguish attenuation anomalies in the upper mantle that have a clearly thermal origin.

Sato & Sacks (1989) and Sato *et al.* (1989) have measured the attenuation in dry peridotite at ultrasonic frequencies (60–900 KHz) in the temperature range $0.95 < T_m/T < 1.17$ (where T_m is solidus temperature) and at pressures of 200–730 MPa. Their assumption of a dry upper-mantle composition is in agreement with recent studies of the electrical conductivity of the stable continental mantle (Hirth *et al.* 2000). The linear dependence of Q_p on the homologous temperature T_m/T (at ultrasonic frequencies) allows extrapolation of the laboratory results to higher pressures through the pressure-dependent solidus temperature $T_m(P)$ (in Kelvin):

$$Q_p = Q_{pm} \exp\{g[T_m(P)/T - a]\}, \tag{5}$$

where $Q_{pm} = 3.5 + P/0.073$ (here P is pressure in GPa), a and g are experimentally determined parameters (a is close to 1, while g is strongly T dependent and increases from 6.75 to 13.3 with an increase of homologous temperature) (Sato *et al.* 1989).

The measurements of Sato *et al.* (1989) were done at ultrasonic frequencies, while mantle attenuation is believed to be strongly frequency dependent (Karato 1998). Romanowicz & Durek (2000) argue that the procedure suggested by Sato *et al.* (1989) to extrapolate their relationship (eq. 5) between Q_p and T_m/T to the seismic frequencies may not be valid, as mechanisms of seismic attenuation other than the grain boundary process assumed by Sato & Sacks (1989) (e.g. dislocation and microcreep processes) can be equally important at seismic conditions (Karato 1998). Nevertheless, eq. (5) permits the making of rough estimates of Q_p from known geotherms, but only in the vicinity of solidus temperatures (*ca* 1200 to 1500 °C). Thus, the approach is not valid for calculations of Q_p^T in the shallow lithosphere or in the cold lithosphere of Precambrian cratons.

Experimental data of Jackson *et al.* (1992) provide basis for estimation of seismic attenuation in a wide temperature range. Their laboratory measurements of attenuation at seismic frequencies (0.01–1 Hz) were made on dry dunite at pressures up to 300 MPa and at temperatures of 20, 600, 800 and 1000 °C. They show that Q_p strongly depends on the oscillation period, τ, and between 600 and 1000 °C increases approximately exponentially with increasing temperature T:

$$1/Q_p = 1/Q_{p0}\tau^{\alpha}, \tag{6}$$

where $1/Q_{p0}$ (i.e. the value of $1/Q_p$ at a 1 s period) exponentially depends on temperature, while the coefficient α is almost temperature independent and may range from 0.15 to 0.30 for different values of τ, T and P. We have approximated the experimental data from Jackson *et al.* (1992) as (T in °C)

$$1/Q_{p0} = \exp(0.00267 * T - 6.765) \tag{7}$$

and have taken $\alpha \sim 0.20$–0.25.

Because the attenuation model based on seismic inversion has the highest resolution at 100 km depth, we focus our analysis at this depth in the upper mantle, for which we compare seismic Q_s with theoretical estimates. We use eqs (6–7) to calculate theoretical values of Q_p^T in the continental upper mantle from temperatures (Artemieva & Mooney 2001) (Fig. 3c). P-wave attenuation, Q_p^T, at a depth of 100 km beneath the continents is calculated from the data on lithospheric temperatures (Artemieva & Mooney 2001) for an oscillation period $\tau = 40$ s and then is converted into Q_s^T values, following the relationship (e.g. Anderson *et al.* 1965)

$$Q_p^{-1} = 4/3 V_s^2/V_p^2 Q_s^{-1} \tag{8}$$

and assuming that for the upper-mantle velocities $Q_p = 2.25\ Q_s$. Because the seismic Q_s model was calculated with respect to the ocean-dominated PREM model, there is a systematic shift of the absolute Q_s values on continents. Thus, the zero anomaly in Fig. 8 (which shows the difference between the seismic Q_s (Fig. 3b) and the Q_s^T values) is centered over the average difference between seismic Q_s and theoretical Q_s^T values, i.e. over $\delta\ Q_s = Q_s - Q_s^T \sim 80$.

5.2 Calculation of theoretical V_s^T at 100 km depth from T

Laboratory measurements of the temperature dependence of density, elastic parameters and, sometimes, direct measurements of the seismic velocities in mantle rocks and rock-forming minerals (Berckhemer *et al.* 1982; Kampfmann & Berckhemer 1985; Sato *et al.* 1989; Jackson *et al.* 1990) provide the basis for estimates of seismic velocities in the upper mantle of a purely thermal origin. A forward

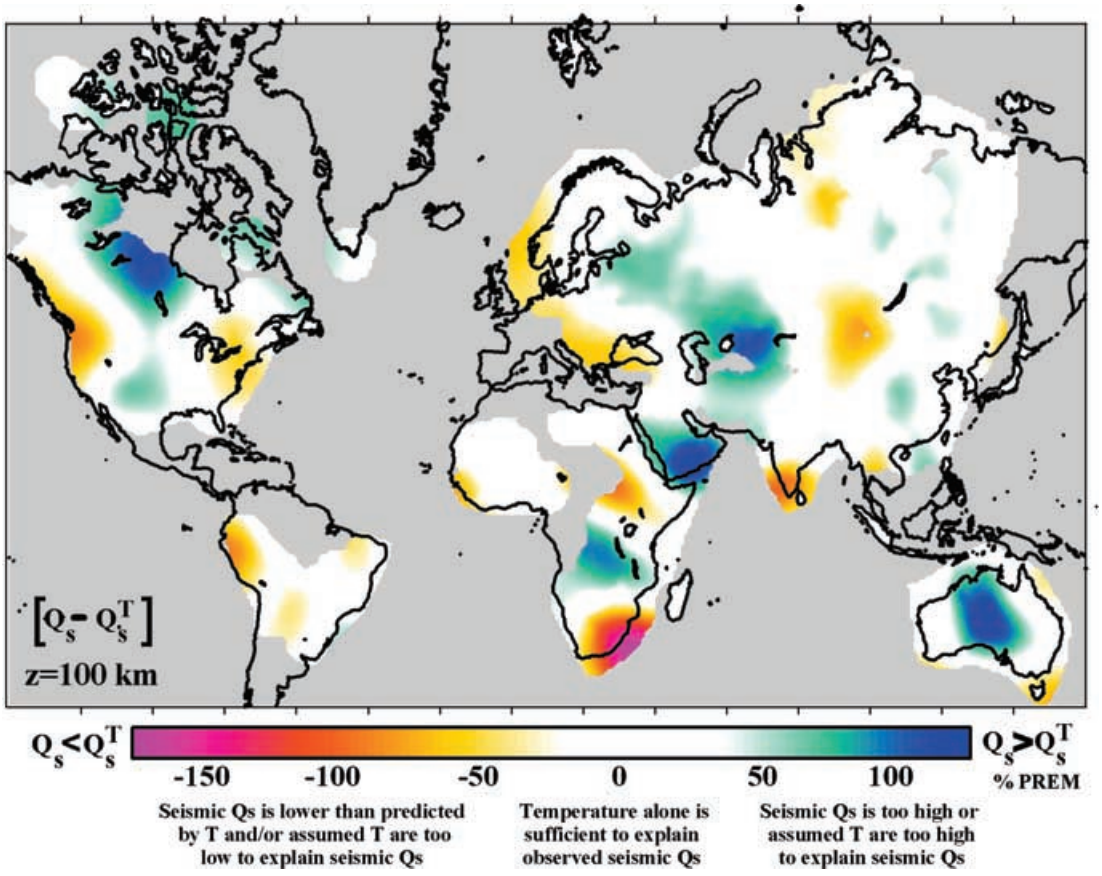

Figure 8. Map of the difference δQ_s between (i) Q_s at 100 km depth as calculated from surface waves (Billien *et al.* 2000) and (ii) the value of Q_s^T estimated from experimental data of Jackson *et al.* (1992) for $\tau = 40$ s and the lithospheric temperatures (Artemieva & Mooney 2001). A large part of the continental lithosphere with diverse ages and tectonic settings fits a purely thermal model for seismic Q_s (white areas). Many active regions appear as more attenuating ($\delta Q_s < 0$), probably as the result of the presence of fluids and partial melts. The anomalies over South Africa and India can be produced by smearing of strong offshore attenuation anomalies. Q_s anomalies in some cratonic regions (central Australia and the Canadian shield) are higher than predicted by Q_s^T models ($\delta Q_s > 0$), suggesting that lithospheric temperatures can be somewhat lower than suggested in Fig. 3(c). Alternative explanation includes scattering on large-scale structural heterogeneities in the cratonic lithosphere, which was formed by collisions of numerous continental and oceanic terranes.

calculation of theoretical V_s^T values from temperature data is free of many uncertainties of inverse modelling of temperatures from seismic V_s because it is not necessary to quantify the effects of composition or the presence of partial melts and fluids on seismic velocities (e.g. Berckhemer *et al.* 1982; Schmeling 1985; Popp & Kern 1993). To calculate theoretical velocities from T (Fig. 3c), we first assume a linear dependence of velocity on temperature with $\partial V_s/\partial T = 0.35$ m s^{-1} K^{-1} (Sumino & Anderson 1982) and for a 100 km depth calculate V_s^T (*elastic*) as velocity anomaly ∂V_s with respect to the PREM value, produced by a temperature variation ∂T with respect to a typical continental geotherm of 55–60 mW m^{-2} (i.e. *ca*1000°C at $z = 100$ km).

In the Earth's mantle, anelasticity significantly affects seismic velocities at seismic frequencies (Karato 1993) and, if not accounted for, can result in overestimated V_s^T anomalies. Because the correlation coefficient between Q_s and V_s calculated in seismic inversion is 0.66 at $z = 100$ km (Section 3), probably partly as a result of the effect of scattering on Q_s, we account for anelasticity as (Minster & Anderson 1981):

$$V_s^T = V_s^T(elastic)[1 - CQ^{-1}(\tau, P, T)], \quad (9)$$

where $C = 2/\tan(\pi\alpha/2)$, $Q^{-1}(\tau, P, T)$ is given by eq. (1) and the numerical values of the parameters are $\alpha = 0.2$, $E^* = 560$ kJ mol^{-1} at $z = 100$ km, and the oscillation period $\tau = 40$ s. Following Sobolev *et al.* (1996), who calibrated the scaling constant A (eq. 1) by fitting average attenuation in the upper mantle by the old ocean geotherm, we take $A = 0.148$.

5.3 Which part of observed variations in seismic Q_s and V_s can be predicted from thermal anomalies alone?

Figs 8–9 show differences δQ_s and δV_s between seismic Q_s and V_s (Figs 3a and b) and theoretical Q_s^T and V_s^T calculated from temperatures (Fig. 3c). Small-scale anomalies result from a different lateral resolution of seismic and temperature models and should be interpreted with caution. Figs 8–9 indicate that in *ca* 50 per cent of the continents seismic attenuation and velocity anomalies can be explained by thermal effects alone (white areas). However, these regions do not show any systematic correlation either with the tectonic setting, or with geological age. Tables 2(a) and (b) provide a summary of the continental regions, where Q_s and V_s anomalies calculated from seismic inversion significantly differ from Q_s^T and V_s^T expected from temperature variations alone. We estimated how much higher (or lower) mantle temperatures should have been to explain the observed $\delta Q_s = Q_s - Q_s^T$ and $\delta V_s = V_s - V_s^T$ misfits. Fig. 10 illustrates how δQ_s and δV_s anomalies were converted into δT anomalies: however, there is a large uncertainty in a conversion of δQ_s anomalies into δT.

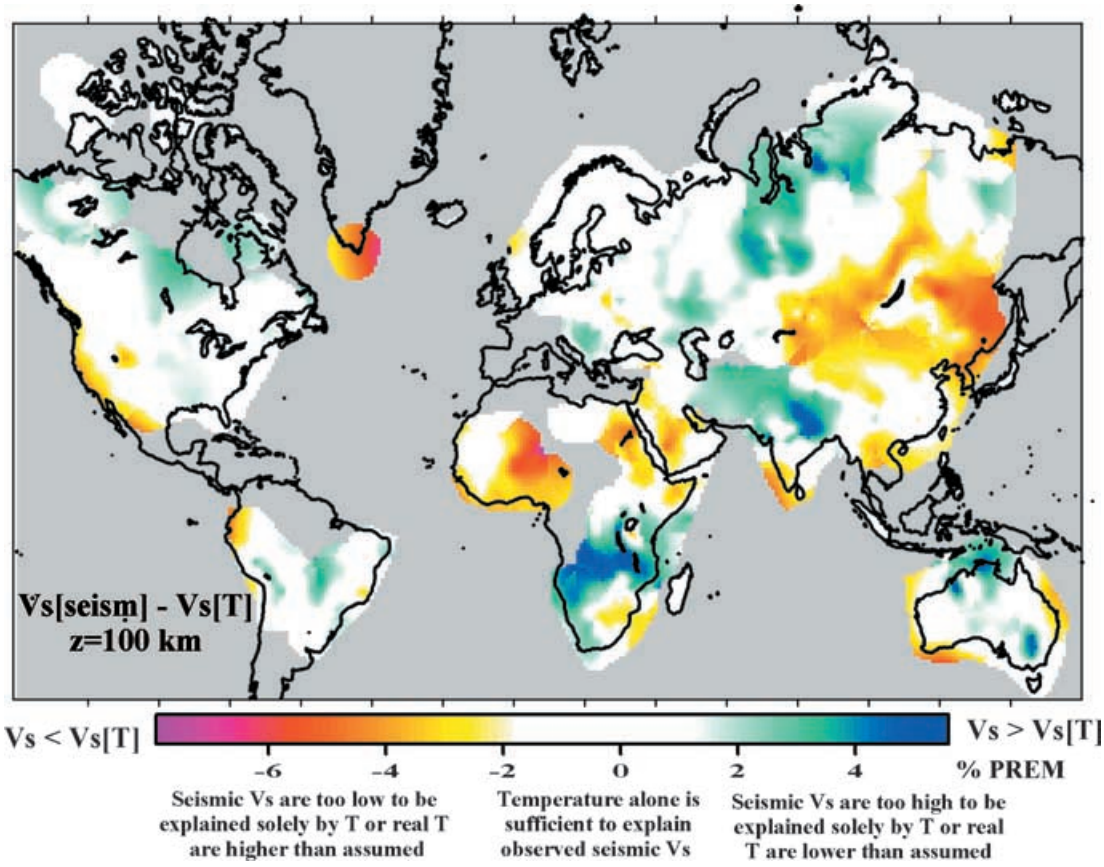

Figure 9. Map of the difference δV_s between (i) V_s at 100 km depth as calculated from surface waves (Billien 1999) and (ii) the value of V_s^T estimated from the lithospheric temperatures (Artemieva & Mooney 2001) with account for anelasticity, for $\tau = 40$ s. Only small areas of the continental lithosphere fit a purely thermal model for seismic V_s (white areas). In many active regions δV_s is *ca* -3 per cent (which corresponds to *ca* 50–70 per cent of the total V_s anomaly), probably as a result of the presence of fluids and partial melts. Positive δV_s anomalies in most of the cratonic regions can be explained by Fe depletion of lithospheric keels. Several Phanerozoic regions have δV_s too large (*ca* 3 per cent) to be explained by overestimated T, these anomalies seem to be associated with past and present subduction zones.

5.3.1 Regions with $Q_s < Q_s^T$ and $V_s < V_s^T$

Red colors in both of the maps (Figs 8–9) outline regions where seismic anomalies could have been explained if upper-mantle T were higher than assumed (Fig. 3c). Surprisingly, there is not much of overlap between the regions with $Q_s < Q_s^T$ and $V_s < V_s^T$ (Table 2a). Areas where seismic V_s are significantly lower than predicted from T (Fig. 9) include mostly tectonically active regions, but negative δQ_s anomalies fall both within active and stable continental regions, suggesting that no single mechanism gives rise to these anomalies. The Arabian shield is the only region where the signs of δQ_s and δV_s anomalies disagree, probably because of a lack of lateral resolution.

Three cratonic regions show negative δQ_s anomalies (Table 2a): however, theoretical velocities well agree there with seismic V_s. Thus, we suggest that seismic Q_s anomalies over the South African and Indian cratons are smearing artefacts of strong offshore attenuation anomalies. We are less certain about the origin of the δQ_s anomaly over a part of the Canadian shield: however, its low amplitude suggests that temperature plays an important role in producing seismic anomalies in all three of these cratonic regions.

The only regions that are red in both of the maps ($\delta Q_s < 0$ and $\delta V_s < 0$) are the western USA and the mountain country of central Asia (Tien-Shan, Sayans and Altai mountains, and Inner Mongolia). These tectonically active regions have a transient thermal regime within the upper mantle and thus temperatures cannot be constrained from a steady-state thermal conductivity equation. Petrologic and non-steady-state geothermal constraints available for these regions (e.g. Lachenbruch & Sass 1977; Polyakov *et al.* 1988; Henry *et al.* 1997; Le Pichon *et al.* 1997) provide constraints on mantle temperatures, but an uncertainty in T values in these regions is much larger than for stable continents. Estimates show that δQ_s and δV_s could be explained if mantle T were above the mantle adiabat, implying that partial melts significantly decrease both Q_s and V_s. This conclusion is supported by regional seismic studies in western USA and Tien Shan (Humphreys & Dueker 1994; Roecker *et al.* 1993) that indicate low seismic velocities in the uppermost mantle and suggest intensive melting at *ca* 100 km depth. Thus, we conclude that all continental regions with reliable constraints on mantle temperatures, where $Q_s > Q_s^T$ and $V_s > V_s^T$, require the presence of partial melt (and/or fluids) in the uppermost mantle to explain observed seismic anomalies.

5.3.2 Regions with $Q_s > Q_s^T$ and $V_s > V_s^T$

There is a striking similarity between the regions with $Q_s > Q_s^T$ and $V_s > V_s^T$ anomalies (Table 2b). Regions where both Q_s and V_s calculated from seismic inversion are higher than expected from

Table 2a. Regions (Figs 8–9) where V_s and Q_s anomalies suggest mantle temperatures higher than assumed (alternative and preferred explanation is a presence of partial melts/fluids).

Regions and T at $z = 100$ km	$\delta V_s = V_s - V_s^T$ (per cent PREM) For V_s^T with account for anelasticity[a]	δT (°C) required to explain δV_s		Regions and T at $z = 100$ km	$\delta Q_s = Q_s - Q_s^T$ (per cent PREM)	δT (°C) required to explain δQ_s
		For δV_s with account for anelasticity[a]	For δV_s from linear V_s–T relationship[b]			
Tien Shan, Altai, Sayans and Inner Mongolia (^) (1100 °C)	−3–4 per cent	+250 °C	+300 °C	Tien Shan, Altai, Sayans and Tarim (^) (1100 °C)	−50–100	Non-defined, in excess of +600 °C
Western North America (*) (^) (1300 °C)	−2–3 per cent	+150 +180 °C	+300 °C	Western North America (**) (^) (1300 °C)	−50–100	Already above adiabat
S Greenland (900 °C)	−4–5 per cent	+250 +300 °C	+500 °C	Abitibi province (Canadian shield) and central part of Grenville province (800–1000 °C)	−50	Non-defined, in excess of +600 °C
Cameroon volcanic line (W Africa) (800 °C) (^^)	−3–4 per cent	+180 +250 °C	+500 °C	South Africa (***) (800–1100 °C)	−150	Non-defined, in excess of +600 °C
Arabian shield and Nubian shield (900–1100 °C)	−3 per cent	+180 °C	+300 +400 °C	Indian shield (***) (800–900 °C)	−150	Non-defined, in excess of +600 °C
S part of the Russian Far East (1100 °C) (^^)	−4–5 per cent	+250 +300 °C	+500 °C	Western part of the Siberian craton (500–700 °C)	−50	+200 +400 °C
				Trans-European Suture Zone (900–1100 °C)	−50	Non-defined, in excess of +600 °C

[a] For V_s^T, δV_s and δT calculated after Deschamps *et al.* (2002).
[b] For V_s^T, δV_s and δT calculated from $\partial V_s / \partial T = 0.35$ m s^{-1} K^{-1}.
^T taken from published petrological and non-steady-state constraints on the thermal regime.
^^No heat flow data, T at the maps is interpolation artefact.
*V_s-to-T conversion used to constrain Fig. 9 can be invalid for this region because of high homologous T.
**Eq. (6) used to constrain Fig. 8 can be invalid for this region because of high homologous T.
***The anomaly most likely is an extension of a strong offshore Q_s anomaly.

Table 2b. Regions (Figs 8–9) where V_s and Q_s anomalies suggest mantle temperatures lower than assumed (alternative and preferred explanation is Fe depletion of cratonic lithosphere).

Regions and T at $z = 100$ km	$\delta V_s = V_s - V_s^T$ (per cent PREM) For V_s^T wiunt for anelasticity[a]	δT (°C) required to explain δV_s		Regions and T at $z = 100$ km	$\delta Q_s = Q_s - Q_s^T$ (per cent PREM)	δT (°C) required to explain δQ_s
		For δV_s with account for anelasticity[a]	For δV_s from linear V_s–T relationship[b]			
East European platform (750–850 °C)	+1 +2 per cent	−70 − 150°C	−100 − 250°C	East European platform (750–850 °C)	+50	−250°C
North and Central Australia (900–1000 °C)	+1 +2 per cent	−70 − 150°C	−100 − 250°C	Central Australia (900–1000 °C)	+150	In excess of −600°C
Slave and Hearne provinces Canadian shield (900 °C)	+1 +2 per cent	−70 − 150°C	−100 − 250°C	Slave and Hearne Provinces (Canadian shield) (900 °C)	+100	−350 − 450°C
South-central USA (900–1000 °C)	+1 per cent	−70°C	−100°C	South-central USA (900–1000 °C)	+50	−250 − 300°C
Mobile belts of South Africa and Central Africa (*) (1200–1300 °C)	+5 per cent	−450°C	−400 − 600°C	Central Africa (**) (1200–1300 °C)	+100	In excess of −600°C
Himalayas and the Tethys belt (*) (ˆ) (1300 °C)	+3 +5 per cent	−250 − 450°C	−250 − 600°C	Himalayas and the Tethys belt (*) (ˆ) (1300 °C)	+50 +100	In excess of −600°C
West Siberia basin and Taimyr peninsula (*) (1100–1300 °C)	+3 +4 per cent	−250 − 350°C	−500 − 600°C	Arabian shield (900–1100 °C)	+150	In excess of −600°C

[a]For V_s^T, δV_s and δT calculated after Deschamps *et al.* (2002).
[b]For V_s^T, δV_s and δT calculated from $\partial V_s/\partial T = 0.35$ m s^{-1} K^{-1}.
ˆT taken from published petrological and non-steady-state constraints on the thermal regime.
*$V_s - T$ conversion used to constrain Fig. 9 can be invalid for this region because of high homologous T.
**Eq. (6) used to constrain Fig. 8 can be invalid for this region because of high homologous T.

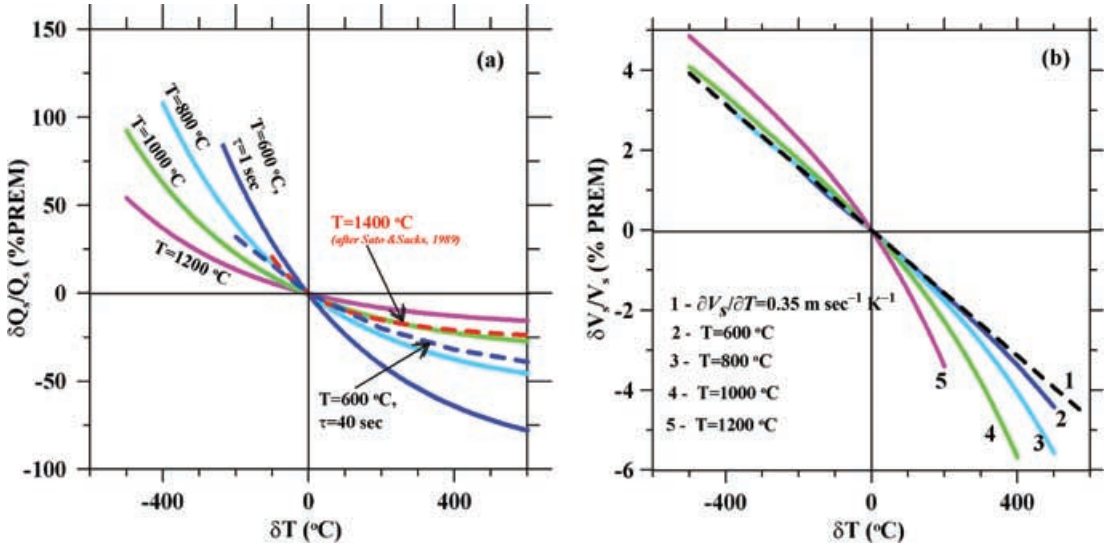

Figure 10. Relative anomalies of Q_s (a) and V_s (b) as a function of T anomalies for different upper-mantle temperatures. (a) Solid lines: δQ_s anomalies based on experimental data of Jackson *et al.* (1992), eqs (6–8), for $\tau = 1$ s. For a comparison, the results for $T = 600$ °C are also presented for $\tau = 40$ s (dashed line). Dashed red line: δQ_s calculated for high homologous mantle T based on experimental data of Sato & Sacks (1989), eq. (5). (b) Solid lines: δV_s anomalies based on eqs (1) and (9), for $\tau = 40$ s. For a comparison, dashed line is δV_s based on a linear relationship $\partial V_s/\partial T = 0.35$ m s^{-1} K^{-1} (Sumino & Anderson 1982).

the conversion of temperature anomalies (shown in blue in Figs 8–9) mostly include Precambrian terranes. Possible explanations for positive δQ_s and δV_s anomalies include overestimated lithospheric temperatures and/or unusually dry conditions within the cratonic lithosphere and/or compositional anomalies. It is surprising that the misfit δV_s between theoretical and seismic V_s is the same in all cratonic regions, *ca* 1–2 per cent. It can be explained by *ca* 70–150 °C lower temperatures at $z = 100$ km than in the T model (Fig. 3c). Alternatively, a typical difference in mg# (MgO/[MgO+FeO]) between the Archean and the Phanerozoic lithosphere (0.93 and 0.89, correspondingly, e.g. Griffin *et al.* 1999) also produces an *ca* 1 per cent velocity anomaly (Deschamps *et al.* 2002). The remaining $\delta V_s < 1$ per cent is within the accuracy of the temperature model. Because it is more uncertain to quantify δT required to explain a δQ_s misfit and the effect of depletion on attenuation is not well known, we are inclined to conclude that δQ_s and δV_s anomalies in the cratonic lithosphere are of a compositional origin (e.g. depletion in basaltic components). This conclusion is supported by recent gravity and buoyancy modelling (e.g. Artemieva 2003; Kaban *et al.* 2003). Given that cratons were formed by collisions of numerous continental and oceanic terranes, their structure can be highly heterogeneous on the lithospheric scale and thus can produce scattering even at frequencies used in the present study, resulting in Q_s and δQ_s anomalies.

A 1 per cent δV_s anomaly in southern USA (southern Great Plain) is within the accuracy of the thermal model: however, it is unlikely that upper-mantle temperatures there are lower than assumed (Fig. 3c). Besides, the region also shows a significant δQ_s anomaly. Recent gravity modelling for North America indicates upper-mantle compositional anomaly in approximately the same region (Mooney & Kaban 2004). Palaeotectonic reconstructions demonstrate that this region has been affected by Palaeozoic subduction (Kluth & Coney 1981). Thus, a possible explanation for δQ_s and δV_s anomalies includes compositional variations in the upper mantle (or fluids).

Other regions where seismic velocities and attenuation cannot be adequately predicted from temperatures include the Himalayas and the Tethys belt in Eurasia and south-central Africa. However, in these regions δQ_s and δV_s anomalies can be biased by the lack of reliable constraints on mantle temperatures. Alternative explanation includes the presence of strong compositional heterogeneities associated with past and present subduction zones in the regions.

The WSB is a region with one of the strongest δV_s anomalies (*ca* 3 per cent), which can be explained only if mantle temperature at $z = 100$ km were *ca* 250 °C lower (i.e. if they were approximately the same as in the Precambrian cratons). Little is known about the ages of the basement rocks in the WSB. However, the entire basin is underlain by a thick layer of basaltic lavas, which have erupted simultaneously with the Siberian traps *ca* 250 Ma (Reichow *et al.* 2002); in late Palaeozoic–Mesozoic time, the basin underwent extensive rifting (Schissel & Smail 2001). Thus, it is likely that the upper mantle of the WSB still has a transient thermal regime and the present surface heat flow does not reflect high mantle temperatures associated with Phanerozoic rifting. This means that actual upper-mantle temperatures in the WSB are likely to be higher, but not lower, than assumed (Fig. 3c). The available data does not permit the making of any further speculations on the origin of a strong δV_s anomaly in WSB, extending to the Taimyr peninsula where Permo-Triassic basalts are also known. However, the results of the recent study of Kaban *et al.* (2003) suggest that there are large compositional differences between the Precambrian lithospheres of the East European platform and the Siberian craton, on one hand, and the Palaeozoic WSB, on the other. Thus, a compositional origin of seismic anomalies in the lithosphere of the WSB cannot be ruled out.

In summary, all positive δQ_s and δV_s anomalies can be explained by compositional variations in the upper mantle. In the cratonic regions, these variations include an Fe depletion of lithospheric keels; in Phanerozoic regions compositional anomalies can be associated

with ancient subduction zones (central Europe, southern USA and the Tethys belt) or may have another unknown non-thermal origin (West Siberian Basin).

6 CONCLUSIONS

Laboratory measurements of seismic velocities and attenuation in upper-mantle rocks show a strong temperature dependence. In this study, we examine the correlations between seismic shear wave velocity, V_s, inverse attenuation, Q_s, and temperature, T, in the continental upper mantle in order to investigate the influence of temperature on V_s and Q_s.

(i) The calculated correlation coefficients, r, between V_s, Q_s and Tanomalies at 50, 100 and 150 km depths do not show a global strong correlation between any pair of parameters. At 100 km depth (where both V_s and Q_s models have high resolution), $r = 0.66$ for Q_s–V_s, $r = -0.56$ for V_s–T, and $r = -0.33$ for Q_s–T. We discuss different physical mechanisms, as well as data modelling artefacts, that can be responsible for a deterioration of global correlations from strong dependencies expected from laboratory measurements. In particular, the poor correlation between temperature and seismic parameters at subcrustal depths may indicate insufficient resolution of temperature constraints. However, the correlation between V_s and Q_s, models derived in the simultaneous inversion of the same data set, is also relatively low. This suggests that the poor correlations can be an intrinsic property of the upper mantle. Prior studies showed that, globally, attenuation and surface heat flow values correlate in the upper 250 km with a low coefficient of $r = 0.20$–0.35 (Romanowicz 1995). We found that for the continental upper mantle the correlation between Q_s and surface heat flow is even less, $r < -0.20$ at $z < 150$ km. Thus, with available data sets we are unable to confirm that temperature is the dominant controlling factor for Q_s and V_s variations on the global scale in the continental upper mantle.

(ii) Because the lateral resolution of our seismic and thermal models differs greatly (*ca* 3000 km vs. 200–1000 km, respectively), this difference in resolution can be partly responsible for low numerical correlations and we visually compare the maps of V_s, Q_s and T for 50, 100 and 150 km depths. Except for the map at 50 km depth (where crustal effects have the strongest effect on V_s and Q_s), we find a good regional qualitative inverse correlation between seismic and thermal parameters. Furthermore, we cannot identify any continental region where both V_s and Q_s do not correlate with T, which would have indicated a clearly non-thermal origin of seismic anomalies. Globally, high V_s, high Q_s and low T correlate with cratons. Thus, in agreement with previous works, we infer that positive seismic anomalies in the cratonic lithosphere are primarily of thermal (low-T) origin. Similarly, we find the expected inverse correlations (low V_s, low Q_s and high T) for many tectonically active regions. We hypothesize that partial melts and/or fluids in the upper mantle of active regions weaken global V_s–T and Q_s–T correlations. The profile along 50°N–60°N, which crosses well-constrained cratonic regions, shows a remarkable correlation between V_s, Q_s and T anomalies. Thus, we conclude that, despite low continent-scale numerical correlations between seismic and thermal anomalies, temperature variations in the upper mantle play an important, but non-unique, role in lateral variations of V_s and Q_s.

(iii) Using laboratory data on the temperature dependence of V_s and Q_s in olivine-rich rocks, we calculate theoretical Q_s^T and V_s^T at $z = 100$ km from known temperatures. A comparison of observed and theoretical values (i.e. $\delta Q_s = Q_s - Q_s^T$ and $\delta V_s = V_s - V_s^T$) provides an estimate of a part of seismic anomalies that cannot be predicted from temperature variations alone. We find that $Q_s < Q_s^T$ and $V_s < V_s^T$ anomalies are observed chiefly in tectonically active regions with high mantle temperatures, where presence of partial melts/fluids may be the cause of very low V_s and Q_s values. However, with few exceptions, regions with $\delta Q_s < 0$ and $\delta V_s < 0$ anomalies do not overlap, suggesting that no single mechanism gives rise to these anomalies. Negative δQ_s and δV_s anomalies could have been explained by higher mantle temperatures. However because the assumed T values are already close to the mantle adiabat, we conclude that a presence of partial melt and/or fluids in the uppermost mantle is required to explain seismic V_s and Q_s. In particular, in active regions partial melts/volatiles may be responsible for δV_s anomalies of *ca* 3 per cent (i.e. > 50–70 per cent of total observed V_s anomalies). Regions with positive δQ_s and δV_s include mostly cratons. A δV_s anomaly of *ca* 1–2 per cent can be explained if temperatures at $z = 100$ km were 70–150 °C lower than assumed. However, we favour compositional origin of seismic anomalies in cratonic lithosphere, because δV_s anomalies can be well explained by a 4 per cent Fe depletion. Several Phanerozoic regions have positive δQ_s and δV_s anomalies, with $\delta V_s \sim 3$ per cent being too large (*ca* 50–70 per cent of V_s anomalies) to be explained by overestimated temperatures. We propose that these δQ_s and δV_s anomalies have a compositional origin and can be associated with ancient subduction zones (central Europe, southern USA, Himalayas and the Tethys belt) or have other unknown non-thermal origin (West Siberian Basin).

This study shows that even if temperature variations in the lithosphere are the main cause of seismic velocity and attenuation variations, other factors, such as presence of melts/fluids and compositional and structural variations, significantly contribute to the observed anomalies in seismic properties. Improved resolution of lithospheric V_s and Q_s is needed to further quantify the factors that control seismic anomalies in the upper mantle.

ACKNOWLEDGMENTS

The authors express their deep gratitude to Jeannot Trampert for his contribution in the calculation of velocity and attenuation models. Discussions with Michel Cara, Jeannot Trampert, Jeroen Ritsema and Saskia Goes provided new insights into the problem. The comments of Karl Fuchs and Hans Thybo on early versions of the manuscript are appreciated. Reviews by Joe Fletcher, Jean-Claude Mareschal and an anonymous reviewer helped to improve the paper.

REFERENCES

Anderson, D.L., 1989. *Theory of the Earth,* Blackwell, Boston, Oxford, p. 366.

Anderson, D.L. & Archambeau, C.B., 1964. The anelasticity of the Earth, *J. geophys. Res.,* **69,** 2071–2084.

Anderson, D.L., Ben-Menahem, A. & Archambeau, C.B., 1965. Attenuation of seismic energy in upper mantle, *J. geophys. Res.,* **70,** 1441–1448.

Artemieva, I.M., 2003. Lithospheric structure, composition, and thermal regime of the East European craton: Implications for the subsidence of the Russian Platform, *Earth planet. Sci. Lett.,* **213,** 429–444.

Artemieva, I.M. & Mooney, W.D., 2001. Thermal structure and evolution of Precambrian lithosphere: A global study, *J. geophys. Res.,* **106,** 16 387–16 414.

BABEL Working Group, 1990. Evidence for early Proterozoic plate tectonics from seismic reflection profiles in the Baltic Shield, *Nature,* **348,** 34–38.

Ben-Menahem, A., 1965. Observed attenuation and Q values of seismic waves in the upper mantle, *J. geophys. Res.,* **70,** 4641–4651.

Berckhemer, H., Kapfmann, W., Aulbach, E. & Schmeling, H., 1982. Shear modulus and Q of forsterite and dunite near partial melting from forced oscillation experiments, *Phys. Earth planet. Int.,* **29,** 30–41.

Bhattacharyya, J.G., Masters, G. & Shearer, P., 1996. Global lateral variations of shear attenuation in the upper mantle, *J. geophys. Res.,* **101,** 22 273–22 290.

Billien, M., 1999. Hétérogénéités de vitesse et d'attenuation du manteau superior à l'echelle globale par modelisation du mode fundamental des ondes de surface, *PhD thesis*, EOST-IPG, Strasbourg.

Billien, M., Lévêque, J.-J. & Trampert, J., 2000. Global maps of Rayleigh wave attenuation for periods between 40 and 150 seconds, *Geophys. Res. Lett.,* **27,** 3619–3622.

Bina, C.R. & Silver, P.G., 1997. Bulk sound travel times and implications for mantle composition and outer core heterogeneity, *Geophys. Res. Lett.,* **24,** 499–502.

Birch, F., 1943. Elasticity of igneous rocks at temperatures and pressures., *Geol. Soc. Am. Bull.,* **54,** 263–286.

Bodri, B., Iizuka, S. & Hayakawa, M., 1991. Relations between deep temperatures and other geophysical characteristics in central Honshu, Japan., *Tectonophysics,* **194,** 325–336.

Boyd, F.R., 1989. Compositional distinction between oceanic and cratonic lithosphere, *Earth planet. Sci. Lett.,* **96,** 15–26.

Canas, J.A. & Mitchell, B.J., 1978. Lateral variation of surface wave anelastic attenuation across the Pacific, *Nature,* **328,** 236–238.

Carlson, R.L. & Miller, D.J., 2003. Mantle wedge water contents estimated from seismic velocities in partially serpentinized peridotites, *Geophys. Res. Lett.,* **30**(5), 1250, doi:10.1029/2002GL016600.

Chan, W.W. & Der, Z.A., 1988. Attenuation of multiple ScS in various parts of the world. Geo, *Phys. J.,* **92,** 303–314.

Christensen, N.I., 1979. Compressional wave velocities in rocks at high temperatures and pressures, critical thermal gradients, and crustal low-velocity zones, *J. geophys. Res.,* **84,** 6849–6857.

Debayle, E. & Kennett, B., 2000. The Australian continental upper mantle: Structure and deformation inferred from surface waves, *J. geophys. Res.,* **105,** 25 423–25 450.

Deschamps, F., Trampert, J. & Snieder, R., 2002. Anomalies of temperature and iron in the uppermost mantle inferred from gravity data and tomographic models, *Phys. Earth planet. Int.,* **129,** 245–264.

Durek, J.J. & Ekström, G., 1996. A radial model of anelasticity consistent with long-period surface-wave attenuation, *Bull. seism. Soc. Am.,* **86,** 144–158.

Durek, J.J., Ritzwoller, M.H. & Woodhouse, J.H., 1993. Constraining upper mantle anelasticity using surface wave amplitude anomalies, *Geophys. J. Int.,* **114,** 249–272.

Dziewonski, A. & Steim, J., 1983. Dispersion and attenuation of mantle waves through waveform inversion, *Geophys. J. R. astr. Soc.,* **70,** 503–527.

Dziewonski, A.M. & Anderson, D.L., 1981. Preliminary reference Earth model., *Phys. Earth planet. Int.,* **2,** 297–356.

Fielitz, K., 1971. Elastic wave velocities in different rocks at high pressure and temperature up to 750 °C, *Z. Geophys.,* **37,** 943–956.

Furlong, F.P., Spakman, W. & Meyer, R.P., 1995. Thermal structure of the continental lithosphere: constraints from seismic tomography., *Tectonophysics,* **244,** 107–117.

Gaal, A. & Gorbatschev, R., 1987. An outline of the Precambrian evolution of the Baltic Shield, *Precambrian Res.,* **35,** 15–52.

Getting, I.C., Dutton, S.J., Burnley, P.C., Karato, S. & Spetzler, H.A., 1997. Shear attenuation in and dispersion in MgO, *Phys. Earth planet. Int.,* **99,** 249–257.

Goes, S. & van der Lee, S., 2002. Thermal structure of the North American uppermost mantle inferred from seismic tomography, *J. geophys. Res.,* **107**(B3), 10.1029/2000JB000049.

Goes, S., Govers, R. & Vacher, P., 2000. Shallow mantle temperatures under Europe from P and S wave tomography, *J. geophys. Res.,* **105,** 11 153–11 169.

Gribb, T.T. & Cooper, R.F., 1998. Low-frequency shear-attenuation in polycrystalline olivine: Grain boundary diffusion and the physical significance of the Andrade model for viscoelastic rheology, *J. geophys. Res.,* **103,** 27 267–27 279.

Griffin, W.L., Zhang, A., O'Reilly, S.Y. & Ryan, C.G., 1998. Phanerozoic evolution of the lithosphere beneath the Sino-Korean craton, in *Mantle Dynamics and Plate Interactions in East Asia*, AGU Geodynam. Monogr., **27**,107–126, eds Flower, M., Chun, S.L., Lo, C.H. & Lee T.Y., AGU, Washington, DC.

Griffin, W.L., O'Reilly, S.Y. & Ryan, C.G., 1999. The composition and origin of subcontinental lithospheric mantle, in, *Mantle Petrology: Field Observations and High Pressure Experimentation: A tribute to Francis R. (Joe) Boyd*, Geochem. Soc. Spec. Publ. No. 6, pp. 13–45, eds Fei, Y., Berthca, C.M. & Mysen, B.O., The Geochemical Society, Houston, TX, USA.

Haapala, N. & Rämö, F., 1991. Petrogenesis of the Proterozoic rapakivi granites of Finland, *Geol. Soc. Am. Spec. Paper,* **24,** 275–286.

Henry, P., Le Pichon, X. & Goffe, B., 1997. Kinematic, thermal and petrological model of the Himalayas: constraints related to metamorphism within the underthrust Indian crust and topographic elevation, *Tectonophysics,* **273,** 31–56.

Hirth, G., Evans, R.L. & Chave, A.D., 2000. Comparison of continental and oceanic mantle electrical conductivity: Is the Archean lithosphere dry?, *Geochem. Geophys. Geosyst.,* **1,** doi 2000GC000048.

Hoshiba, M., 1993. Separation of scattering attenuation and intrinsic absorption in Japan using the multi lapse time window analysis of full seismogram envelope, *J. geophys. Res.,* **98,** 15 809–15 824.

Huang, Z., Su, W., Peng, Y., Zheng, Y. & Li, H., 2003. Rayleigh wave tomography of China and adjacent regions, *J. geophys. Res.,* **108**(B2), 2073, doi:10.1029/2001JB001696.

Hughes, D.S. & Cross, J.H., 1951. Elastic wave velocities at high pressures and temperatures, *Geophysics,* **16,** 577–593.

Humphreys, E.D. & Dueker, K.G., 1994. Physical state of the western U.S. upper mantle, *J. geophys. Res.,* **99,** 9635–9650.

Ide, J.M., 1937. The velocity of sound in rocks and glasses as a function of temperature, *J. Geol.,* **45,** 689–716.

Jackson, I., 1993. Progress in the experimental study of seismic wave attenuation, *Ann. Rev. Earth planet. Sci.,* **21,** 375–406.

Jackson, I., 2000. Laboratory measurement of seismic wave dispersion and attenuation: recent progress, *Geophys. Monogr.,* **117,** 265–289.

Jackson, I. & Rigden, S.M., , 1998. Composition and temperature of the Earth's mantle: seismological models interpreted through experimental studies of Earth materials. in *The Earth's Mantle: Composition, Structure and Evolution*, pp. 405–460, ed. Jackson I., Cambridge Univ. Press, New York.

Jackson, I., Rudnick, R.L., O'Reilly, S.Y. & Bezant, C., 1990. Measured and calculated elastic wave velocities for xenoliths from the lower crust and upper mantle, *Tectonophysics,* **173,** 207–210.

Jackson, I., Paterson, M.S. & Fitz Gerald, J.D., 1992. Seismic wave dispersion and attenuation in Åheim dunite: an experimental study, *Geophys. J. Int.,* **108,** 517–534.

Jackson, I., Fitz Gerald, J.D., Faul, U.H. & Tan, B.H., 2002. Grain-size-sensitive seismic wave attenuation in polycrystalline olivine., *J. geophys. Res.,* **107**(B12), 2360, doi: 10.1029.2001JB001225.

Jaupart, C., 1983. Horizontal heat transfer due to radioactivity contrasts: Causes and consequences of the linear heat flow relation, *Geophys. J. R. astr. Soc.,* **75,** 411–435.

Jaupart, C. & Mareschal, J.-C., 1999. The thermal structure and thickness of continental roots, *Lithos,* **48,** 93–114.

Jones, A.G., 1984. The electrical structure of the lithosphere and asthenosphere beneath the Fennoscandian Shield, *J. Geomag. Geoelectr.,* **35,** 811–827.

Jones, A.G., 1999. Imaging the continental upper mantle using electromagnetic methods, *Lithos,* **48,** 57–80.

Kaban, M.K., Schwintzer, P., Artemieva, I.M. & Mooney, W.D., 2003. Density of continental roots: compositional and thermal effects, *Earth planet. Sci. Lett.,* **209,** 53–69.

Kampfmann, W. & Berckhemer, H., 1985. High temperature experiments on the elastic and anelastic behaviour of magmatic rocks, *Phys. Earth planet. Int.,* **40,** 223–247.

Karato, S.-I., 1990. Low Q zone at the base of the mantle: Evidence for lower mantle convection?, *Phys. Earth planet. Int.,* **22,** 155–161.

Karato, S.-I., 1993. Importance of anelasticity in the interpretation of seismic tomography, *Geophys. Res. Lett.,* **20,** 1623–1626.

Karato, S.-I., 1998. A dislocation model of seismic wave attenuation and micro-creep in the earth: Harold Jeffreys and the rheology of the solid Earth, *Pure appl. Geophys.,* **153**(2–4), 239–256.

Karato, S.I. & Spetzler, H.A., 1990. Effect of microdynamics in minerals and solid-state mechanisms of seismic wave attenuation and velocity dispersion in the mantle, *Rev. Geophys.,* **28,** 399–421.

Kern, H., 1978. The effect of high temperature and high confining pressure on compositional wave velocities in quartz-bearing and quartz-free igneous and metamorphic rocks, *Tectonophysics,* **44,** 185–203.

Kluth, C.F. & Coney, P.J., 1981. Plate tectonics of the ancestral Rocky Mountains, *Geology,* **9,** 10–15.

Lachenbruch, A.H. & Sass, J.H., 1977. Heat flow in the United States and the thermal regime of the crust, *Geophys. Monogr. Ser.,* **20,** 626–675.

Le Pichon, X., Henry, P. & Goffe, B., 1997. Uplift of Tibet: from eclogites to granulites—implications for the Andean Plateau and the Variscan belt, *Tectonophysics,* **273,** 57–76.

Minster, J.B. & Anderson, D.L., 1981. A model of dislocation-controlled rheology for the mantle, *Phil. Trans. R. Soc. Lond.*,A.**299,** 319–-356.

Mitchell, B.J., 1995. Anelastic structure and evolution of the continental crust and upper mantle from seismic surface wave attenuation, *Rev. Geophys.,* **33,** 441–462.

Mitchell, B.J., Pan, Y., Xie, J. & Cong, L., 1997. Lg coda Q variation across Eurasia and its relation to crustal evolution, *J. geophys. Res.,* **102,** 22 767–22 779.

Mooney, W.D. & Kaban, M.K., 2004. Density structure and evolution of the North American upper mantle, *J. geophys. Res.,* submitted

Mooney, W.D., Laske, G. & Masters, T.G., 1998. CRUST 5.1: A global crustal model at 5° × 5°, *J. geophys. Res.,* **103,** 727–747.

Murase, T. & Fukuyama, H., 1980. *Shear Wave Velocity in Partially Molten Peridotite at High Pressures*, Year Book Carnegie Institute, Washington, DC, **79,** pp. 307–310.

Murase, T. & Kushiro, I., 1979. *Compressional Wave Velocity in Partially Molten Peridotite at High PressuresM*, Year Book Carnegie Institute, Washington, DC, **78,** pp. 559–562.

Nakajima, J. & Hasegawa, A., 2003. Estimation of thermal structure in the mantle wedge of northeatsren Japan from seismic attenuation data, *Geophys. Res. Lett.,* **30**(14), 1760, doi:10.1029/2003GL017185.

Nakanishi, I., 1978. Regional difference in the phase velocity and the quality factor Q of mantle Rayleigh waves, *Science,* **200,** 1379–1381.

Neumann, E.-R., Olsen, K.H. & Baldridge, W.S., 1995. The Oslo Rift, in, *Continental Rifts: Evolution, Structure, Tectonics*, pp. 345–374, ed. Olsen, K.H., Elsevier, Amsterdam, the Netherlands.

Nolet, G. & Zielhuis, A., 1994. Low S velocities under the Tornquist-Teisseyre zone: Evidence from water injection into the transition zone by subduction, *J. geophys. Res.,* **99,** 15 813–15 820.

Pollack, H.N. & Chapman, D.S., 1977. On the regional variation of heat flow, geotherms and lithospheric thickness, *Tectonophysics,* **38,** 279–296.

Pollack, H.N., Hurter, S.J. & Johnson, J.R., 1993. Heat flow from the Earth's interior: analysis of the global data set, *Rev. Geophys.,* **31,** 267–280.

Polyakov, A.I., Muravieva, N.S. & Senin, V.G., 1988. Partial melting of the upper mantle in the Baikal rift (from studies of glasses in lherzolite nodules and megachrysts), *Doklady Akad. Nauk SSSR,* **300**(1), 208–213 (in Russian).

Popp, T. & Kern, H., 1993. Thermal hydration reaction characterized by combined measurements of electrical conductivity and elastic wave velocities, *Earth planet. Sci. Lett.,* **120,** 43–57.

Reichow, M.K., Saunders, A.D., White, R.V., Pringle, M.S., Al'Mukhamedov, A.I., Medvedev, A.I. & Kirda, N.P., 2002. $^{40}Ar/^{39}Ar$ dates from the West Siberian Basin: Siberian flood basalt province doubled, *Science,* **296,** 1846–1849.

Reid, F.J.L., Woodhouse, J.H. & van Heijst, H.J., 2001. Upper mantle attenuation and velocity structure from measurements of differential S phases, *Geophys. J. Int.,* **145,** 615–630.

Roecker, S.W., Sabitova, T.M., Vinnik, L.P., Burmakov, Y.A., Golvanov, M.I., Mamatkanova, R. & Munirova, L., 1993. Three-dimensional elastic wave velocity structure of the Western and Central Tien Shan, *J. geophys. Res.,* **98,** 15 779–15 795.

Romanowicz, B., 1994. Anelastic tomography: a new perspective on upper-mantle thermal structure, *Earth planet. Sci. Lett.,* **128,** 113–121.

Romanowicz, B., 1995. A global tomographic model of shear attenuation in the upper mantle, *J. geophys. Res.,* **100,** 12 375–12 394.

Romanowicz, B. & Durek, J.J., 2000. Seismological constraints on attenuation in the Earth: review, *Geophys. Monogr.,* **117,** 161–178.

Roth, E.G., Wiens, D.A. & Zhao, D., 2000. An empirical relationship between seismic attenuation and velocity anomalies in the upper mantle, *Geophys. Res. Lett.,* **27,** 601–604.

Roult, G., 1982. The effect of young oceanic regions on the periods and damping of free oscillations of the Earth, *J. Geophys.,* **51,** 38–43.

Sarker, G. & Abers, G.A., 1998. Deep structures along the boundary of a collisional belt: attenuation tomography of P and S waves in the Greater Caucasus, *Geophys. J. Int.,* **133,** 326–340.

Sarker, G. & Abers, G.A., 1999. Lithospheric temperature estimates from seismic attenuation across range fronts in southern and central Eurasia, *Geology,* **27,** 427–430.

Sato, H. & Sacks, I.S., 1989. Anelasticity and thermal structure of the oceanic mantle: Temperature calibration with heat flow data, *J. geophys. Res.,* **94,** 5705–5715.

Sato, H., Sacks, I.S., Murase, T., Muncill, G. & Fukuyama, H., 1989. Q_p-melting temperature relation in peridotite at high pressure and temperature: Attenuation mechanism and implications for the mechanical properties of the upper mantle, *J. geophys. Res.,* **94,** 10 647–10 661.

Sato, H.I., Sacks, E., Takahashi, E. & Scarfe, C.M., 1988. Geotherms in the Pacific Ocean from laboratory and seismic attenuation studies, *Nature,* **336,** 154–156.

Schissel, D. & Smail, R., 2001. in *Mantle Plumes: their Identification through Time*, 291–322, eds Ernst, R.E., et al Geol. Soc. Am., Boulder, CO.

Schmeling, H., 1985. Numerical models on the influence of partial melt on elastic, anelastic and electric properties of rocks. Part 1. Elasticity and anelasticity, *Phys. Earth planet. Int.,* **41,** 34–57.

Selby, N.D. & Woodhouse, J.H., 2002. The Q structure of the upper mantle: Constraints from Rayleigh wave amplitudes, *J. geophys. Res.,* **107(5)**,2001JB000257.

Sheehan, A.F. & Solomon, S.C., 1992. Differential shear wave attenuation and its lateral variation in the North Atlantic region, *J. geophys. Res.,* **97,** 15 339–15 350.

Simons, F.J., Zielhuis, A. & van der Hilst, R.D., 1999. The deep structure of the Australian continent from surface wave tomography, *Lithos,* **48,** 17–43.

Sobolev, S.V., Zeyen, H., Stoll, G., Werling, F., Altherr, R. & Fuchs, K., 1996. Upper mantle temperatures from teleseismic tomography of French Massif Central including effects of composition, mineral reactions, anharmonicity, anelasticity and partial melt, *Earth planet. Sci. Lett.,* **139,** 147–163.

Su, W.-J., Woodward, R.L. & Dziewonski, A.M., 1994. Degree-12 model of shear velocity heterogeneity in the mantle, *J. geophys. Res.,* **99,** 6945–6980.

Sumino, Y. & Anderson, O.L., 1982. Elastic constants in minerals, in, *CRC Handbook of Physical Properties of Rocks*, pp. 39–138, ed. Carmichel, R.S., CRC Press, Boca Raton, FL.

Tan, B.H., Jackson, I. & Fitz Gerald, J.D., 1997. Shear wave dispersion and attenuation in fine-grained synthetic olivine aggregates: preliminary results, *Geophys. Res. Lett.,* **24,** 1055–1058.

Tarantola, A. & Valette, B., 1982. Generalized nonlinear inverse problems solved using the least squares inversion, *Rev. Geophys.,* **20,** 219–232.

Trampert, J. & Woodhouse, J.H., 1995. Global phase velocity maps of Love and Rayleigh waves between 40 and 150 s, *Geophys. J. Int.,* **122,** 675–690.

Trampert, J. & Woodhouse, J.H., 2001. Assessment of global phase velocity models, *Geophys. J. Int.,* **144,** 165–174.

Trampert, J. & Woodhouse, J.H., 2003. Global anisotropic phase velocity maps for fundamental mode surface waves between 40 and 150 s., *Geophys. J. Int.,* **154,** 154–165.

Tsumura, N., Matsumoto, S., Horiuchi, S. & Hasegawa, A., 2000. Three-dimensional attenuation structure beneath the northeastern Japan arc estimated from spectra of small earthquakes, *Tectonophysics,* **319,** 241–260.

Woodhouse, J.H. & Wong, Y.K., 1986. Amplitude, phase and path anomalies of mantle waves, *Geophys. J. R. astr. Soc.,* **87,** 753–773.

Xu, X., O'Reilly, S.Y., Griffin, W.L. & Zhou, X., 2000. Genesis of young lithospheric mantle in southeastern China; an LAM-ICPMS trace element study., *J. Petrol.,* **41,** 111–148.